IMMUNOLOGY

# Differential metabolic requirement governed by transcription factor c-Maf dictates innate γδT17 effector functionality in mice and humans

**Xu Chen[1,2], Yihua Cai[2], Xiaoling Hu[2], Chuanlin Ding[2], Liqing He[3], Xiang Zhang[3], Fuxiang Chen[1,4]*, Jun Yan[2]***



**Cellular metabolism has been proposed to govern distinct γδ T cell effector functions, but the underlying molecular mechanisms remain unclear. We show that interleukin-17 (IL-17)–producing γδ T (γδT17) and interferon-γ (IFN-γ)–producing γδ T (γδT1) cells have differential metabolic requirements and that the rate-limiting enzyme isocitrate dehydrogenase 2 (IDH2) acts as a metabolic checkpoint for their effector functions. Intriguingly, the transcription factor c-Maf regulates γδT17 effector function through direct regulation of IDH2 promoter activity. Moreover, mTORC2 affects the expression of c-Maf and IDH2 and subsequent IL-17 production in γδ T cells. Deletion of c-Maf in γδ T cells reduces metastatic lung cancer development, suggesting c-Maf as a potential target for cancer immune therapy. We show that c-Maf also controls IL-17 production in human γδ T cells from peripheral blood and in oral cancers. These results demonstrate a critical role of the transcription factor c-Maf in regulating γδT17 effector function through IDH2-mediated metabolic reprogramming.**

## INTRODUCTION

γδ T cells play a critical role in tissue homeostasis and host defense against pathogens in both mice and humans (*1*–*3*). Preprogrammed in the thymus, γδ T cells can mainly divide into interleukin-17 (IL-17)–producing γδ T cells (γδT17) and interferon-γ (IFN-γ)–producing counterpart (γδT1) based on their cytokine secretion profiles (*4*). γδT17 display proinflammatory function in infectious diseases, autoimmune disorders, and tumor microenvironment (*2*, *5*, *6*). Murine γδT17 (mostly restricted to $Vγ4^+$ and $Vγ6^+$, Heilig and Tonegawa's system) lack CD27, CD73, or CD45RB but express CCR6, IL-1 receptor (IL-1R), and IL-23R, whereas human γδT17 (including $Vδ1^+$ and $Vδ2^+$) express CCR6, CD161, and natural killer receptors (*7*–*12*). A complex of regulatory network integrating environmental cues, cellular intrinsic signaling, and transcription factors governs the development and effector function of γδ T subsets (*13*–*15*). In mice, cytokines and Notch and T cell receptor (TCR) signaling pathways play critical roles in the development and function of γδT17 (*16*). Precisely, IL-1β/IL-1R, IL-23/IL-23R, and spleen tyrosine kinase/phosphatidylinositol 3-kinase/Akt pathway regulate the production of IL-17 in mouse γδ T cells (*10*, *17*, *18*). However, limited information has been known about human γδT17. Previous studies have shown that a cocktail of cytokines and transcription factors such as retinoic acid-related orphan receptor gamma t (RORγt) or signal transducer and activator of transcription 3 (STAT3) are required for human γδT17 differentiation and function (*9*, *19*–*21*). Recently, it has been revealed that the activator protein-1 (AP-1) transcription factor c-Maf acts as a universal commitment factor that drives type 17 programming in all murine γδ T subsets via coordinating with RORγt and RORγt-independent molecular mechanisms (*7*). RORγt is also expressed in human γδT17, and targeting RORγt in spondyloarthritis inhibits the function of human γδT17 (*20*). However, the role of c-Maf in human γδT17 and its potential in human disease remains unclear.

Transcription factor–mediated molecular signals usually work with metabolic programming for cellular function (*22*–*24*). Cellular metabolism has emerged as the key regulator for T cell proliferation, differentiation, and function (*25*–*27*). Recently, it has been reported that γδT1 and γδT17 subsets have distinct metabolic requirements (*28*–*30*). γδT1 are dependent on glycolysis, and glucose supplement enhances the antitumor function of γδT1 cells, while γδT17 engage oxidative phosphorylation (OXPHOS) metabolism (*28*) and glutamine metabolism (*29*, *30*). Dermal γδT17 also rely on OXPHOS pathway and glutaminolysis, and the mechanistic or mammalian target of rapamycin (mTOR) signaling and STAT3 are essential for dermal γδT17 effector functions (*31*, *32*). Moreover, mTOR complex 1 (mTORC1) was required for the survival of peripheral $Vγ4^+$ subset, and loss of Raptor-mediated mTORC1 signaling promotes γδ T generation (*33*, *34*), while targeting mTORC2 signaling significantly reduces imiquimod-induced skin inflammation (*31*). However, it remains elusive how the transcription factor–mediated cellular metabolic complex network coordinates in γδ T cells, e.g., the role of c-Maf in regulating γδT17 metabolism. Here, we show that γδT17 and γδT1 are regulated through different metabolic pathways, and the transcription factor c-Maf serves as a key orchestrator of cellular metabolism in γδT17. Specifically, c-Maf directly regulates the rate-limiting metabolic enzyme isocitrate dehydrogenase 2 (IDH2) and interacts with the mTORC2 signaling in γδT17 to regulate its effector function.

## RESULTS

### Differential metabolic pathways used by $CD27^-$ γδ and $CD27^+$ γδ T cell subsets

Specialized metabolic pathways link to differential T effector subsets (*35*). CD27 is a functional marker to differentiate IFN-γ–producing

[1]Department of Clinical Immunology, Shanghai Ninth People's Hospital, Shanghai Jiao Tong University School of Medicine, Shanghai, China. [2]Division of Immunotherapy, The Hiram C. Polk, Jr., MD Department of Surgery, Immuno-Oncology Program, Brown Cancer Center, University of Louisville School of Medicine, Louisville, KY, USA. [3]Department of Chemistry, University of Louisville, Louisville, KY, USA. [4]Faculty of Medical Laboratory Science, Shanghai Jiao Tong University School of Medicine, Shanghai, China.
*Corresponding author. Email: jun.yan@louisville.edu (J.Y.); fuxiang_chen@hotmail.com (F.C.)

γδ T cells (CD27$^+$ γδT1) from IL-17–producing γδ cells (CD27$^-$ γδT17) (*4*). We then explored the metabolic differences between CD27$^-$ γδT17 and CD27$^+$ γδT1 effector cells. Using in vitro polarized CD27$^+$ and CD27$^-$ γδ T cells, we first verified the distinct cytokine production in these two subsets (fig. S1, A to D). We found that CD27$^+$ γδT1 expressed higher *glucose transporter 1* (*Glut1*) mRNA and had more glucose uptake compared to CD27$^-$ γδT17 as determined by 2-NBDG (2-(*N*-(7-nitrobenz-2-oxa-1,3-diazol-4-yl)amino)-2-deoxyglucose) uptake (Fig. 1, A and B), suggesting that CD27$^+$ γδT1 may predominately use glycolytic metabolic pathway for energy fuel. In contrast, CD27$^-$ γδT17 expressed higher metabolic enzymes such as *glutaminase* (*GLS*) and *glutamate dehydrogenase 1* (*GLUD1*) in glutamine metabolism compared to CD27$^+$ γδT1 cells (Fig. 1C), while glutamine transporter CD98 expression showed no difference (fig. S1E), implying that CD27$^-$ γδT17 may also depend on glutaminolysis.

Previous studies have shown that γδT17 mainly use the OXPHOS pathway (*31*), suggesting the importance of the tricarboxylic acid (TCA) cycle in γδT17 cells. To further unbiasedly profile γδ T cell metabolic pathways, we cultured CD27$^+$ γδT1 and CD27$^-$ γδT17 cells with $^{13}$C-labeled glucose for stable isotope-resolved metabolomics (SIRM) analysis (Fig. 1D). The total differentially expressed metabolites related to glycolysis and the TCA cycle between these two subsets of γδ T cells are shown in fig. S1F. CD27$^+$ γδT1 cells showed increased, labeled isotopologs including pyruvate and lactate, suggesting that glycolysis dominated metabolic pathway (Fig. 1D and fig. S1G). In contrast, CD27$^-$ γδT17 cells had increased, labeled isotopologs such as cis-aconitate, α-ketoglutaric acid (α-KG), malate, and glutamate that are mainly involved in the TCA cycle (Fig. 1D and fig. S1G), further supporting the possibility of differential metabolic activities between CD27$^-$ γδT17 and CD27$^+$ γδT1 effectors. Because OXPHOS takes place in the mitochondria, we then examined mitochondrial function in CD27$^-$ and CD27$^+$ γδ T cells by MitoTracker Green/Red staining. There was not much difference in intact and dysfunctional mitochondria between these two subsets (Fig. 1E). However, a much higher level of mitochondrial reactive oxygen species (mitoROS) was detected in CD27$^+$ γδT1 by mitoSOX Red staining (Fig. 1F), and this phenotype was not the consequence of cell size difference as two subsets showed similar sizes (Fig. 1F). In addition, inhibition of ROS significantly reduced IFN-γ production from CD27$^+$ γδT1 cells (fig. S2A), suggesting a critical role of ROS in CD27$^+$ γδT1 effector function. We also observed that CD27$^+$ γδT1 cells were prone to apoptosis induction upon TCR stimulation, while there was no impact on CD27$^-$ γδT17 cells (fig. S2B). Together, these data suggest that distinct metabolism and mitochondrial function are present between CD27$^-$ γδT17 and CD27$^+$ γδT1 effectors.

## CD27$^-$ γδ and CD27$^+$ γδ T cell effector function is governed by differential metabolic pathways

To validate the role of differential metabolism in CD27$^-$ γδT17 and CD27$^+$ γδT1 effector functions, we used small-molecule inhibitors to block different metabolic pathways and examine their influence on cytokine production. Polarized CD27$^-$ γδ T cells predominately secreted IL-17, while CD27$^+$ γδ T cells mainly produced IFN-γ (Fig. 2A). 2-Deoxy-D-glucose (2-DG) is a glucose analog that acts to competitively inhibit the glucose metabolism. After 2-DG treatment, CD27$^-$ γδT17 cells showed no difference in IL-17 production, while CD27$^+$ γδT1 exhibited a great decrease in IFN-γ production in a dose-dependent manner (Fig. 2B). By targeting pyruvate kinase (PK) with oxalate (OXA), both CD27$^-$ γδT17 and CD27$^+$ γδT1 reduced cytokine production, suggesting a common metabolic pathway in these two subsets (Fig. 2C). Inhibition of the enzyme IDH by AGI also decreased the production of cytokines in CD27$^-$ and CD27$^+$ γδ T (Fig. 2D), indicating the significant role of metabolic enzymes such as IDH in γδ T functions. Collectively, differential and shared metabolic pathways are required for the effector function of CD27$^-$ γδT17 and CD27$^+$ γδT1 subsets.

## IDH2 serves as the metabolic checkpoint for γδ T effector function

Rate-limiting enzymes play pivotal roles in the metabolic pathways. We next examined the expression of a series of metabolic enzymes that are involved in glycolysis and TCA cycle, including hexokinase 1 (HK1), pyruvate dehydrogenase kinase 1 (PDK1), pyruvate kinase M2 (PKM2), lactate dehydrogenase A (LDHA), IDH1, and IDH2 between two subsets of γδ T cells. We found that IDH2, which is an enzyme in mitochondria catalyzing the oxidative decarboxylation of isocitrate and producing α-KG, was expressed higher in CD27$^-$ γδT17 cells as compared to CD27$^+$ γδT1 cells. This was revealed by both Western blot (Fig. 3A) and real-time polymerase chain reaction (RT-PCR) analyses (Fig. 3B). We also analyzed other TCA-related enzymes and found that fumarase, succinate dehydrogenase complex flavoprotein subunit A, and mitochondrial pyruvate carrier 1 were noticeably stronger in CD27$^-$ γδT17 than those in CD27$^+$ γδT1 cells (fig. S2C), further supporting the notion that CD27$^-$ γδT17 cells preferentially use OXPHOS metabolism. $^{13}$C-labeled tracing experiment showed that the transformation to α-KG from (iso)citrate was substantially decreased in CD27$^+$ γδT1 cells compared to CD27$^-$ γδT17 cells, suggesting that there is a metabolic break from citrate to α-KG flow in these cells (Fig. 3, C and D). To demonstrate the precise role of IDH2 in regulating differential γδ T effector functions, IDH2 in CD27$^-$ γδT17 was silenced by small interfering RNA (siRNA) interference, and we found that IL-17 production was significantly decreased in CD27$^-$ γδT17 regardless of the stimulators (Fig. 3E). In addition, the mRNA expression levels of *c-Maf* and *Rorc* were also significantly reduced upon IDH2 siRNA treatment (Fig. 3F). In contrast, upon gain of function of IDH2 in CD27$^+$ γδT1 by lentivirus transfection, we found the decrease of IFN-γ production (Fig. 3G). Furthermore, addition of α-KG into the medium also dampened the production of IFN-γ in CD27$^+$ γδT1 cells (Fig. 3H). These data demonstrate that IDH2 serves as the metabolic checkpoint for effector function in γδ T cells.

## Transcription factor c-Maf regulates IDH2 activity to orchestrate IL-17 production in γδ T cells

The transcription factor c-Maf was reported to be specifically expressed in primary CD27$^-$ γδT17 and progenitors (*7*). We confirmed the expression of c-Maf in polarized CD27$^-$ γδT17 cells but not in CD27$^+$ γδT1 cells by flow cytometry (Fig. 4A) and RT-PCR analysis (Fig. 4B). Upon c-Maf–specific inhibitor nivalenol (NIV) treatment, CD27$^-$ γδT17 cells had reduced mRNA expression levels of *c-Maf*, *RORγt*, and *IDH2* and attenuated production of IL-17 (Fig. 4C). To rule out any off target effect of c-Maf inhibitor NIV, we generated Rorc-cre; c-Maf$^{f/f}$ mice. The c-Maf expression was completely abrogated in CD27$^-$ γδT17 from Rorc-cre; c-Maf$^{f/f}$ mice (Fig. 4D). Consistent with c-Maf inhibitor data, we also saw significantly decreased IDH2 mRNA expression level in CD27$^-$ γδT17 from Rorc-cre; c-Maf$^{f/f}$ mice (Fig. 4E). However, the mRNA expression

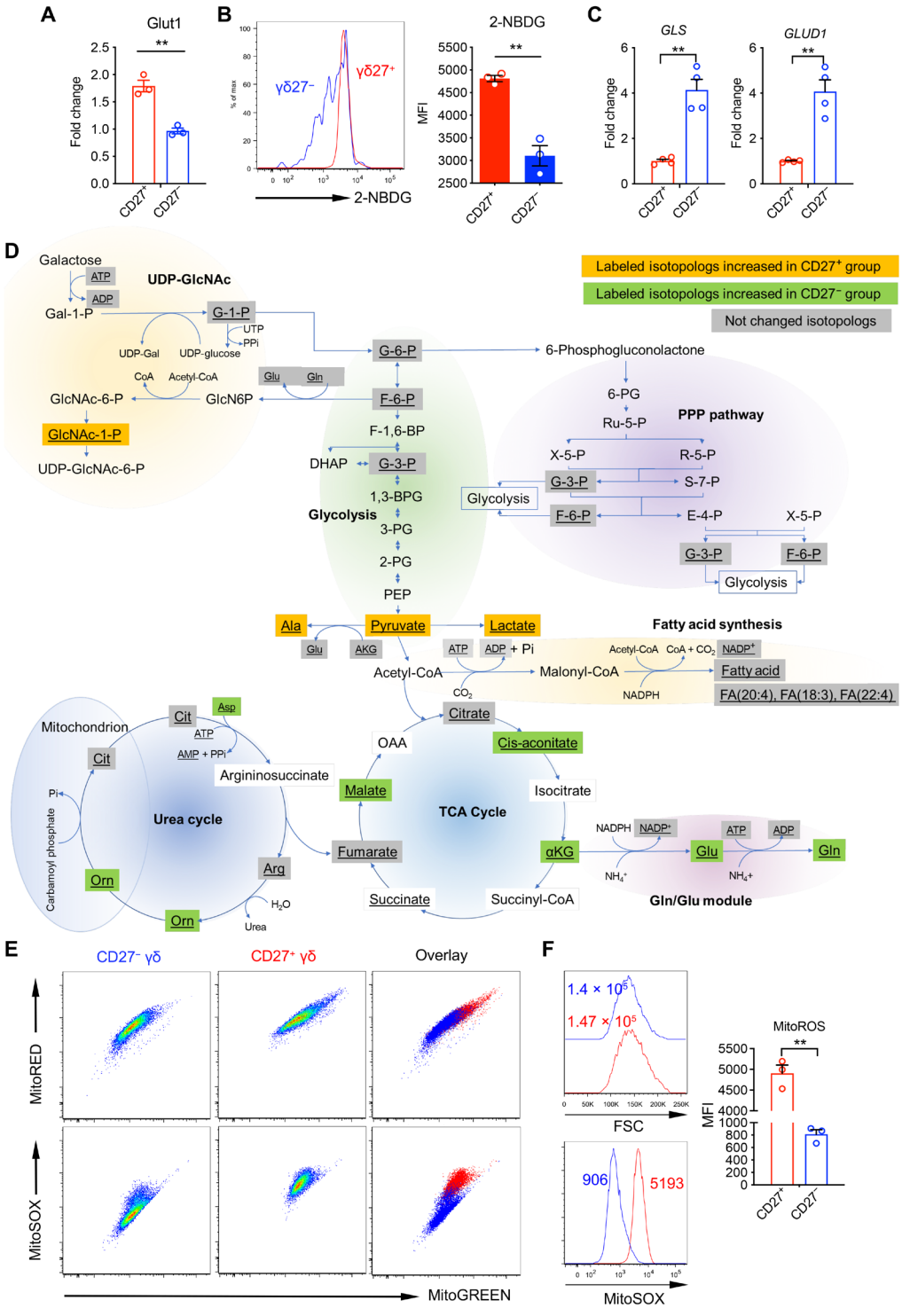


**Fig. 1. Differential metabolic requirement for CD27$^+$ and CD27$^-$ γδ T cells.** (**A**) The mRNA expression levels of *Glut1* in polarized CD27$^+$ and CD27$^-$ γδ T cells by real-time polymerase chain reaction (RT-PCR). (**B**) 2-NBDG uptake in polarized CD27$^+$ and CD27$^-$ γδ T cells assessed by flow cytometry. Representative histogram and summarized mean fluorescence intensity (MFI) data are shown. (**C**) The mRNA expression levels of *GLS* and *GLUD1* in polarized CD27$^+$ and CD27$^-$ γδ T cells. (**D**) Differential abundance of metabolites detected by SIRM in polarized CD27$^-$ ($n = 5$) and CD27$^+$ ($n = 6$) γδ T cells. (**E**) MitoGREEN/MitoRED (top) and MitoGREEN/MitoSOX (bottom) staining of polarized CD27$^-$ and CD27$^+$ γδ T cells. Representative dot plots are shown. (**F**) Cell size [forward scatter (FSC)] from polarized CD27$^-$ and CD27$^+$ γδ T (top) and MitoSOX staining from polarized CD27$^-$ and CD27$^+$ γδ T (bottom). Summarized data of mitochondrial ROS from polarized CD27$^-$ and CD27$^+$ γδ T are shown (right). Data are represented as means ± SEM. $^{**}P < 0.01$. Data (A to C and E to F) are representative of at least three independent experiments with similar results. AMP, adenosine 5′-monophosphate; ATP, adenosine 5′-triphosphate; ADP, adenosine 5′-diphosphate; CoA, coenzyme A; DHAP, dihydroxyacetone phosphate; NADP$^+$, nicotinamide adenine dinucleotide phosphate; NADPH, reduced form of NADP$^+$; PEP, phosphoenolpyruvate; PPP, pentose phosphate pathway; PPi, inorganic pyrophosphate; UDP, uridine 5′-diphosphate.

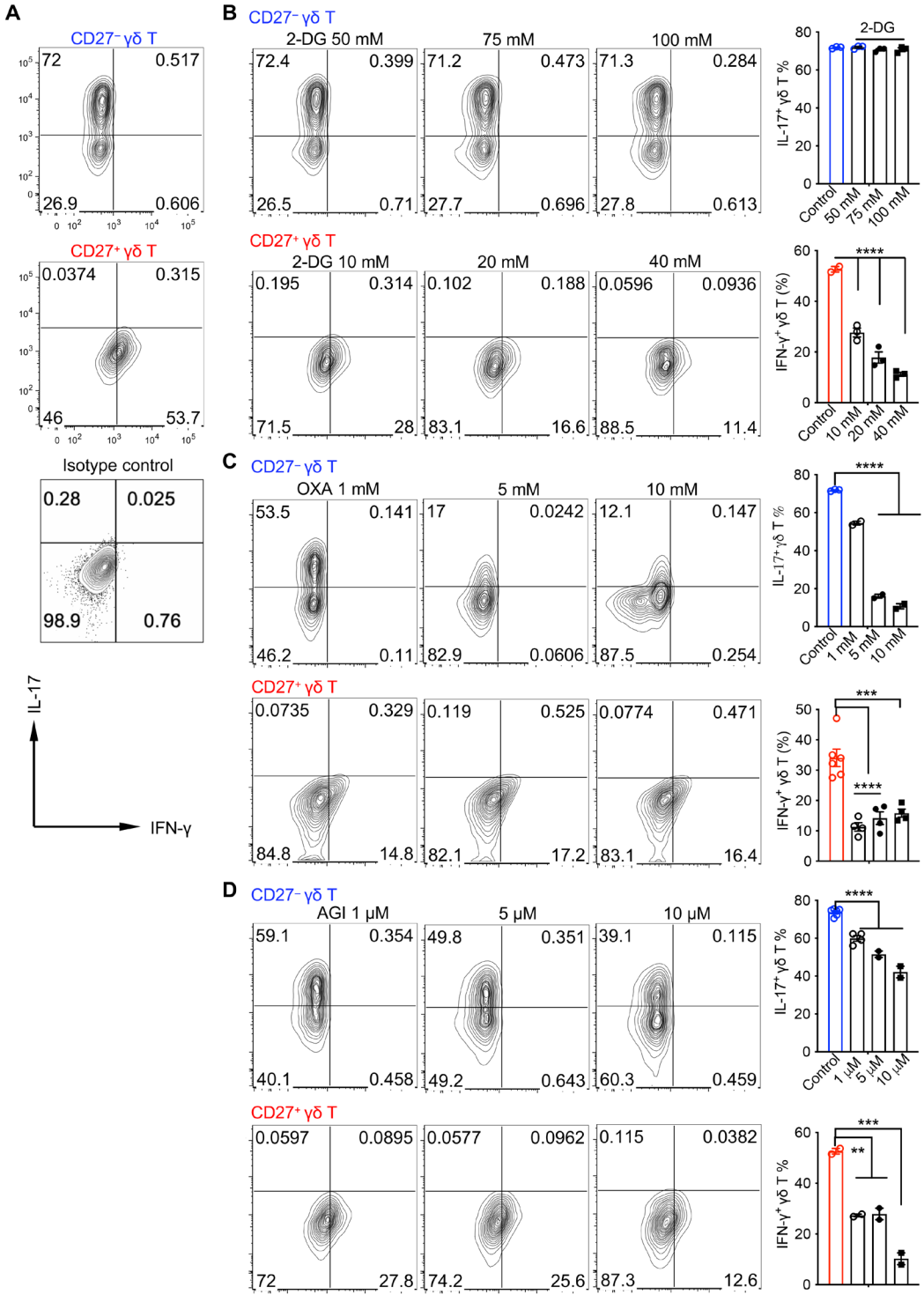


**Fig. 2. Inhibition of metabolic pathways affects the cytokine production of CD27$^+$ and CD27$^-$ γδ T cells.** (**A**) Cytokine profiles of polarized CD27$^+$ (top) and CD27$^-$ (middle) γδ T cells. Isotype control for IFN-γ staining is shown in the bottom. (**B**) 2-DG was added into the cell culture, and intracellular IL-17 (top) and IFN-γ (bottom) were measured. Representative dot plots and summarized data are shown. (**C**) Cell cultures were added with various concentrations of OXA, and intracellular IL-17 and IFN-γ were measured. Representative dot plots and summarized data are shown. (**D**) Various concentrations of AGI were added into the cell culture, and intracellular IL-17 and IFN-γ were measured. Representative dot plots and summarized data are shown. Data are represented as means ± SEM. $^{**}P < 0.01$, $^{***}P < 0.001$, and $^{****}P < 0.0001$. Data are representative of at least three independent experiments with similar results.

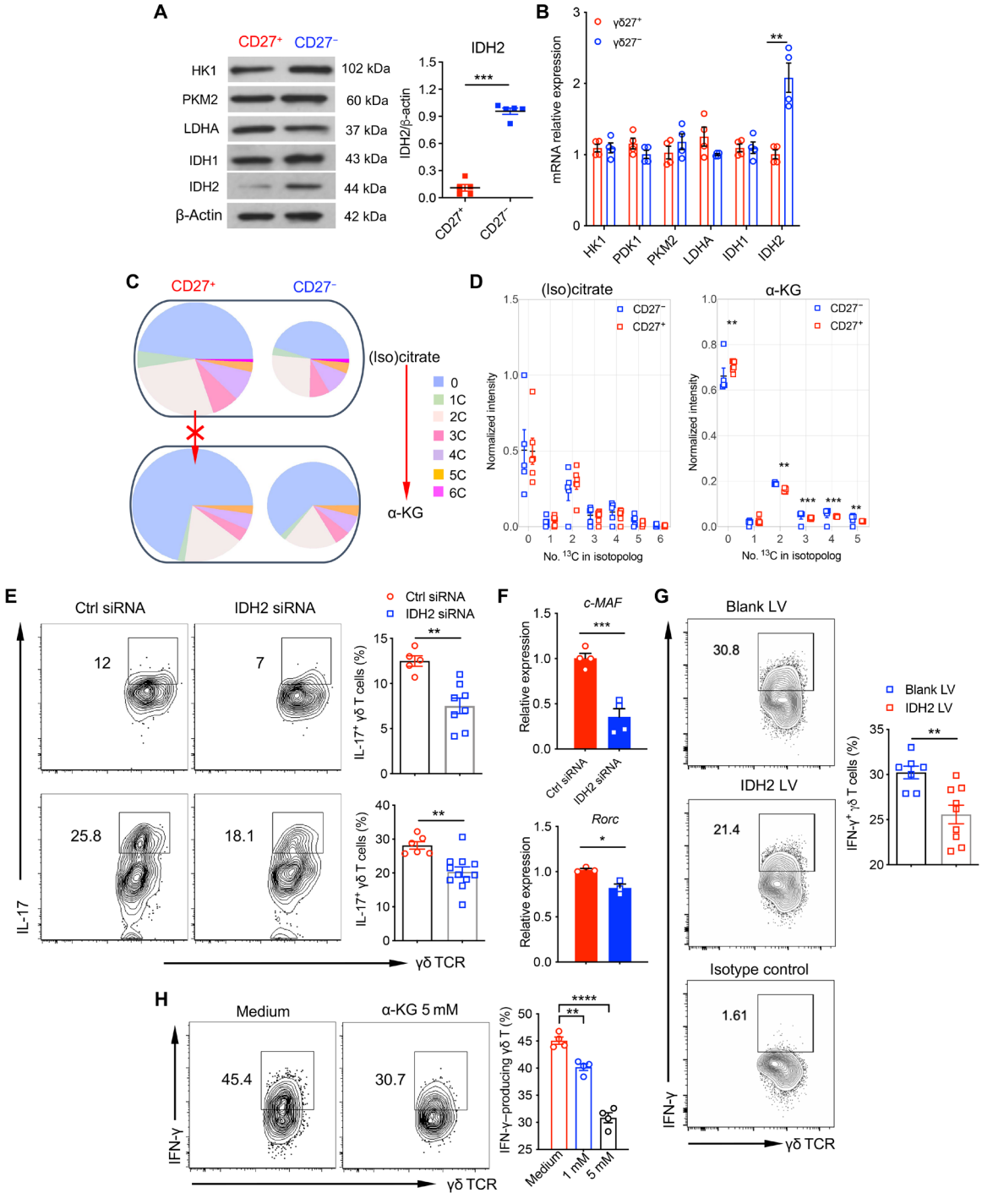


**Fig. 3. IDH2 serves as a metabolic checkpoint for CD27$^+$ and CD27$^-$ γδ T cells.** (**A**) Western blot analysis of metabolic enzymes including HK1, PKM2, LDHA, IDH1, and IDH2 in polarized CD27$^+$ and CD27$^-$ γδ T cells (left). Quantitative densitometry analysis on IDH2 expression (right). (**B**) The mRNA expression levels of *HK1*, *PDK1*, *PKM2*, *LDHA*, *IDH1*, and *IDH2* in polarized CD27$^+$ and CD27$^-$ γδ T cells. (**C**) $^{13}$C-labeled glucose tracing experiment in polarized CD27$^+$ and CD27$^-$ γδ T cells. Pie charts show $^{13}$C-labeled and unlabeled (iso)citrate and α-KG in CD27$^+$ and CD27$^-$ γδ T cells. (**D**) Relative intensity of $^{13}$C labeled and unlabeled (iso)citrate and α-KG in polarized CD27$^+$ ($n = 6$) and CD27$^-$ γδ T cells ($n = 5$). (**E**) Polarized CD27$^-$ γδ T cells were transfected with control (Ctrl) or IDH2 siRNA and then stimulated with IL-1β and IL-23 (top panel) or phorbol 12-myristate 13-acetate (PMA) and ionomycin (bottom panel). Intracellular IL-17 was detected by flow cytometry. Representative dot plots and summarized data are shown. (**F**) The mRNA expression levels of *c-MAF* and *Rorc* in control or IDH2 siRNA-transfected polarized CD27$^-$ γδ T cells. (**G**) Polarized CD27$^+$ γδ T cells were infected with blank lentivirus (LV) or IDH2-expressing lentivirus and then stimulated with PMA and ionomycin. Intracellular IFN-γ was detected. Isotype control for IFN-γ staining is also shown. Representative dot plots and summarized data are shown. (**H**) Polarized CD27$^+$ γδ T cells were cultured in the presence or absence of α-KG and then stimulated by PMA and ionomycin for intracellular IFN-γ production. Representative dot plots and summarized data are shown. Data are represented as means ± SEM. *$P < 0.05$, **$P < 0.01$, ***$P < 0.0001$, and ****$P < 0.0001$.

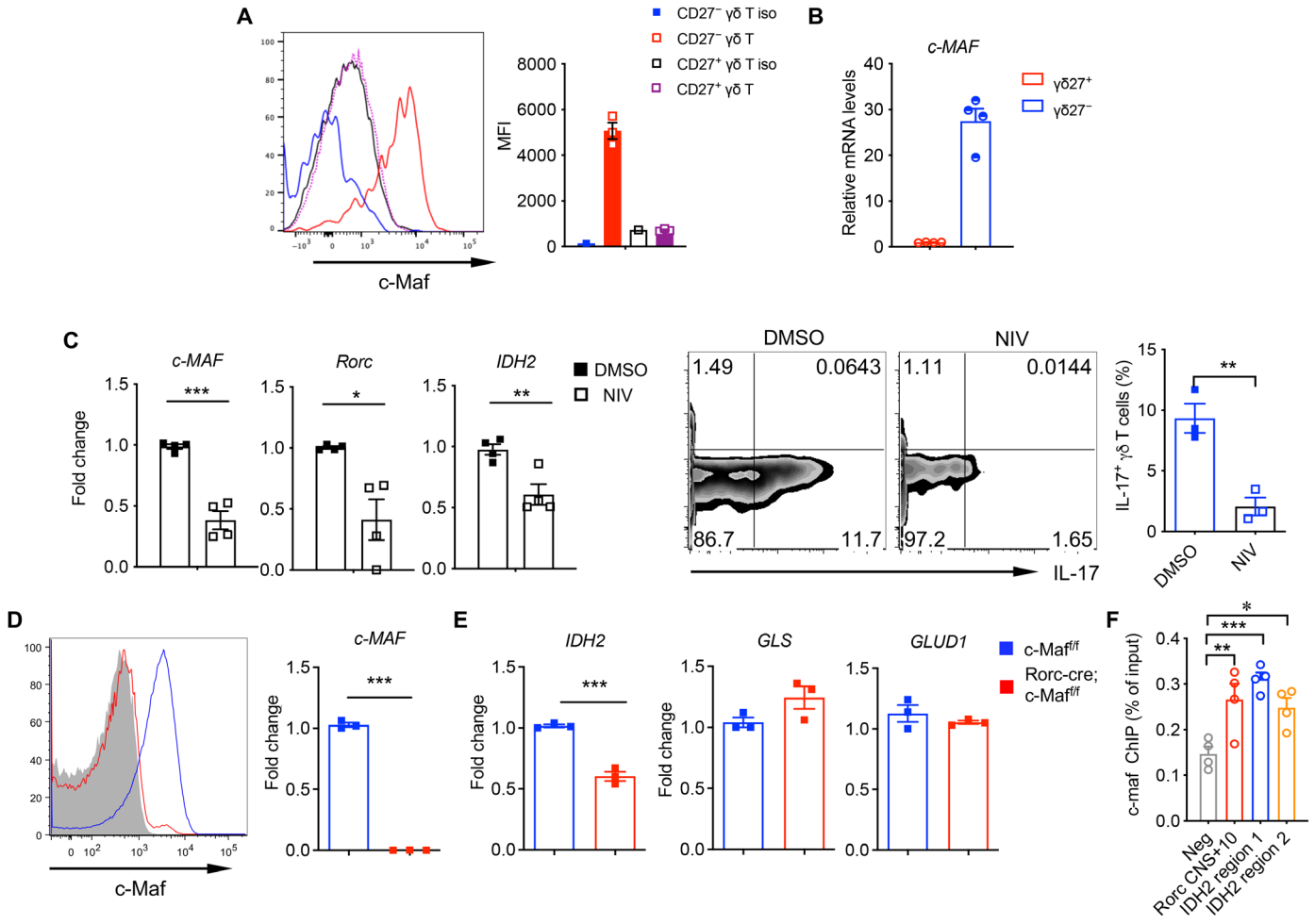


**Fig. 4. Transcription factor c-Maf regulates IDH2 activity in CD27⁻ γδ T cells.** (**A**) The c-Maf expression in polarized CD27⁺ and CD27⁻ γδ T cells assessed by flow cytometry. Representative histogram and summarized MFI are shown. (**B**) The c-Maf mRNA expression in polarized CD27⁺ and CD27⁻ γδ T cells by RT-PCR analysis. (**C**) Polarized CD27⁻ γδ T cells were treated with dimethyl sulfoxide (DMSO) or c-Maf inhibitor NIV, and the mRNA levels of c-Maf, Rorc, and IDH2 were assayed by RT-PCR analysis. Cells were also stimulated with IL-1β and IL-23, and intracellular IL-17 production was measured by flow cytometry. Representative flow plots and summarized data are shown. (**D**) c-Maf expression in polarized CD27⁻ γδ T cells from c-Maf$^{f/f}$ (blue) or Rorc-cre; c-Maf$^{f/f}$ (red) mice by flow cytometry (left) or by RT-PCR analysis (right). (**E**) The mRNA expression level of *IDH2*, *GLS*, and *Glud1* in polarized CD27⁻ γδ T cells from c-Maf$^{f/f}$ or Rorc-cre; c-Maf$^{f/f}$ mice. (**F**) ChIP-qPCR analysis of predictive c-Maf binding sites in IDH2, including two IDH2 regions: a negative control and a positive control (Rorc CNS+10). Data are represented as means ± SEM. **P* < 0.05, ***P* < 0.01, and ****P* < 0.001. Data (A to E) are representative of at least three independent experiments with similar results.

levels of *GLS* and *Glud1* were not altered (Fig. 4E). To further determine the underlying mechanism, we performed a virtual screening to see whether c-Maf could bind to the promoter region of IDH2. We found that c-Maf has two binding sites on the IDH2 promoter region. To confirm this, we performed c-Maf chromatin immunoprecipitation (ChIP) and then examined IDH2 promoter activity. As shown in Fig. 4F, c-Maf directly bound onto two predicted regions in IDH2 promoter as assessed by ChIP–quantitative PCR (qPCR) analysis. As expected, c-Maf also bound to Rorc promoter region as previously reported (*7*). Together, these data suggest that transcription factor c-Maf directly regulates IDH2 activity via binding to IDH2 promoter region.

## The mTORC2 pathway affects the c-Maf expression in γδT17 cells

We next explored the potential signaling pathways that regulate c-Maf expression. The mTOR pathway is a critical regulator linking metabolism and molecular signaling (*36*, *37*). We previously discovered that mTORC2 but not mTORC1 affected the IL-17 production in dermal γδ T cells (*31*). Here, we confirmed that loss of function in Rictor-mediated mTORC2 signaling (fig. S3A), but not Raptor-mediated mTORC1 signaling (fig. S4A), led to reduced IL-17 production in γδ T from inguinal lymph nodes (iLNs). In contrast, γδT1 cell function was not affected by mTORC2 deficiency. Similarly, IL-17 production of lung γδ T but not γδT1 cells were also greatly decreased after depletion of Rictor in γδ T cells (fig. S3A). Furthermore, the percentage of lung CD27⁻ γδ T cells decreased (fig. S3B). In addition, Vγ4 T cells were also significantly decreased in CD27⁻ γδ T cells from CD2-cre; Rictor$^{f/f}$ conditional knockout (cKO) mice (fig. S3C). Rictor deficiency in γδ T cells also led to the reduced c-Maf expression in lung γδ T cells (fig. S3D). Because c-Maf directly regulates IDH2 activity as shown above, we then examined IDH2 expression level in CD27⁻ γδT17 cells. As shown in fig. S3E, IDH2 expression level was substantially reduced in

Rictor-deficient CD27$^-$ γδ T cells as compared to CD27$^-$ γδ T cells from control mice assessed by Western blot analysis (left) and RT-PCR analysis (right). These results reveal that the mTORC2 has a regulatory role in c-Maf, thus controlling IL-17 production in γδ T cells.

Hypoxia-inducible factor 1α (HIF-1α) is essential for T helper cell 17 ($T_H17$) generation and differentiation (*24*, *38*), and higher mRNA expression of HIF-1α was also detected in CD27$^-$ γδT17 cells (fig. S4B). However, there was no significant difference in γδ T cell numbers from iLNs, spleens, and the lungs of control versus HIF-1α cKO mice (fig. S4C). In addition, neither γδ T cell production of IL-17 and IFN-γ (fig. S4D) nor c-Maf expression in γδ T cells was altered in HIF-1α cKO mice (fig. S4E). These results suggest that HIF-1α is dispensable for γδT17 effector function. Together, these data indicate that the mTORC2 signaling, not mTORC1 or HIF-1α, regulates CD27$^-$ γδT17 effector function through the c-Maf–IDH2 axis.

### c-Maf deficiency in γδ T cells reduces metastatic lung cancer

Lung γδT17 cells have been reported to play a critical role in promoting metastatic lung cancer (*39*). We next examined the role of c-Maf in metastatic lung cancer development and progression. To this end, Rorc-cre; c-Maf$^{f/f}$ mice and control mice were injected intravenously with green fluorescent protein (GFP)–tagged Lewis lung carcinoma (LLC) cells. Fourteen days after tumor cell injection, mice were euthanized, and tumor burden was determined by flow cytometry. We found significantly decreased LLC tumor cells in the lungs of Rorc-cre; c-Maf$^{f/f}$ mice (Fig. 5A) compared to control mice. In addition, tumor-bearing Rorc-cre; c-Maf$^{f/f}$ mice had prolonged survival compared to control mice (Fig. 5B). We also examined the immunophenotype of the lungs. As shown in Fig. 5C, the percentages of lung γδ T, particularly γδT17, were greatly decreased, while IFN-γ–producing γδT1 cells were significantly elevated in Rorc-cre; c-Maf$^{f/f}$ mice compared to those in control mice. However, there were no differences in the production of IFN-γ in CD4$^+$ and CD8$^+$ T cells (Fig. 5D). Unexpectedly, IL-17 production in CD4$^+$ T cells was slightly increased (Fig. 5D). Furthermore, there was no substantial difference regarding the total CD45$^+$ pan immune cells and CD11b$^+$ myeloid cells (Fig. 5E) in the lungs between these two strains of mice. We further used metastatic melanoma B16F10 model to validate these findings. As shown in Fig. 5F, B16F10 lung metastasis model also indicated a prolonged survival in Rorc-cre; c-Maf$^{f/f}$ mice compared to control mice. These results demonstrate the critical role of γδT17 cells in metastatic lung cancer and imply c-Maf as a potential target for cancer immunotherapy.

### c-Maf controls γδT17 in humans and is correlated with oral cancer progression

Transcription factor c-Maf has been shown to regulate γδT17 in mice, while its role in human γδT17 remains undefined. In healthy individuals, the percentage of γδ T from peripheral blood was less than 10%, and these γδ T cells consisted mainly Vδ2 (*40*). The primary γδ T cells in the peripheral blood secreted a negligible level of IL-17 but mainly produced IFN-γ (fig. S5A). It has been reported that human γδT17 cells express CCR6 (*12*) but only a small proportion of CCR6$^+$ γδ T cells (γδT$^{CCR6+}$) in the periphery. We then used a previously described protocol to polarize human γδT17 (*41*). The γδ T cells expanded and produced more IL-17 after polarization, and IL-17–producing γδ T cells were restricted to CCR6$^+$ subsets, while CCR6$^-$ γδ T cells secreted scarce amount of IL-17 (Fig. 6A). In addition, the *IL-17A* mRNA was also highly expressed in γδT$^{CCR6+}$ compared to γδT$^{CCR6-}$ (Fig. 6B). IDH2 siRNA interference significantly decreased IL-17 production in γδT$^{CCR6+}$ (Fig. 6C and fig. S5B). We also observed that c-Maf was highly expressed in γδT$^{CCR6+}$ at both the protein and mRNA levels (Fig. 6D). Inhibition of c-Maf with NIV, human γδT$^{CCR6+}$ showed decreased IL-17 production (Fig. 6E), similar to their mouse counterparts (Fig. 4C).

To examine the regulation of γδT17 in human diseases, we recruited patients with oral squamous cell carcinoma (OSCC). We found a significant amount of γδ T cell infiltration in OSCC tissues, and a fraction of γδ T cells expressed CCR6 (fig. S5C). Similarly, these CCR6$^+$ γδ T cells from OSCC also secreted a considerable amount of IL-17 (Fig. 7A). Inhibition of IDH2 with small-molecule inhibitor AGI significantly decreased IL-17 production in CCR6$^+$ γδ T cells from patients with OSCC (fig. S5D). To further explore different clusters of γδ T cells in human OSCC tissues, we performed a single-cell RNA sequencing (scRNA-seq) using two pairs of tumor and adjacent tissues. By scRNA-seq, we discovered diverse immune cells (fig. S5E) and different clusters of T cells (fig. S5F) in normal adjacent tissue (N) and OSCC tissue (T). Using uniform manifold approximation and projection (UMAP) and conventional γδ T cell lineage genes, we identified five different clusters of γδ T cells in human oral tissues (Fig. 7B). Cluster analysis for each pair is shown in fig. S5G. Of which, clusters 1 and 4 showed high expression of *IFNG* and *TBX21*, which is transcription factor for $T_H1$ cells compared to other clusters (Fig. 7C), indicating γδT1 phenotype. Notably, cluster 5 (Fig. 7B, black dotted circle) expressed higher levels of *c-MAF*, *CCR6*, *IL-17A*, and *IL-22* while lower levels of *IFNG* and *TBX21* than other clusters (Fig. 7C), indicating that this cluster represents human γδT17 cells. Cluster 2 also expressed high levels of *MAF* and *CCR6*, but *IL-17A* and *RORC* levels were low, suggesting that this cluster may be precursors of cluster 5 as shown in pseudotime analysis (fig. S5H). Compared to γδ T cells in normal adjacent oral tissues (Fig. 7B), OSCC tissues had more abundant γδT17 cells (cluster 5). Further metabolism-related gene expression profile revealed that IDH1 and IDH2 in cluster 5 were highly expressed in OSCC tissue compared to these in an adjacent tissue (Fig. 7D). In contrast, IDH1 and IDH2 expression levels in cluster 1 were decreased in OSCC tissue compared to normal adjacent tissue. Using publicly available datasets, we found that patients with head neck squamous carcinoma (HNSC) whose tumors had low c-Maf expression with high γδ T cell infiltration exhibited a significant better overall survival compared to other combinations (Fig. 7E). These data suggest a critical role of c-Maf–mediated metabolic reprogramming in human γδT17 cells and further support the notion that targeting c-Maf in γδ T may provide benefit for treating patients with cancer.

## DISCUSSION

γδ T cells are innate-like lymphocytes existing in the peripheral blood and mucosal tissues. While γδT1 cells show potent antitumor function, γδT17-mediated protumor effects have been observed in both human cancers and murine tumor models (*39*, *42*–*45*). Cellular metabolism plays a central role in the function of T cells, and distinct metabolic requirements between γδT1 and γδT17 cells have been reported (*28*). γδT1 cells are mainly dependent on glycolysis,

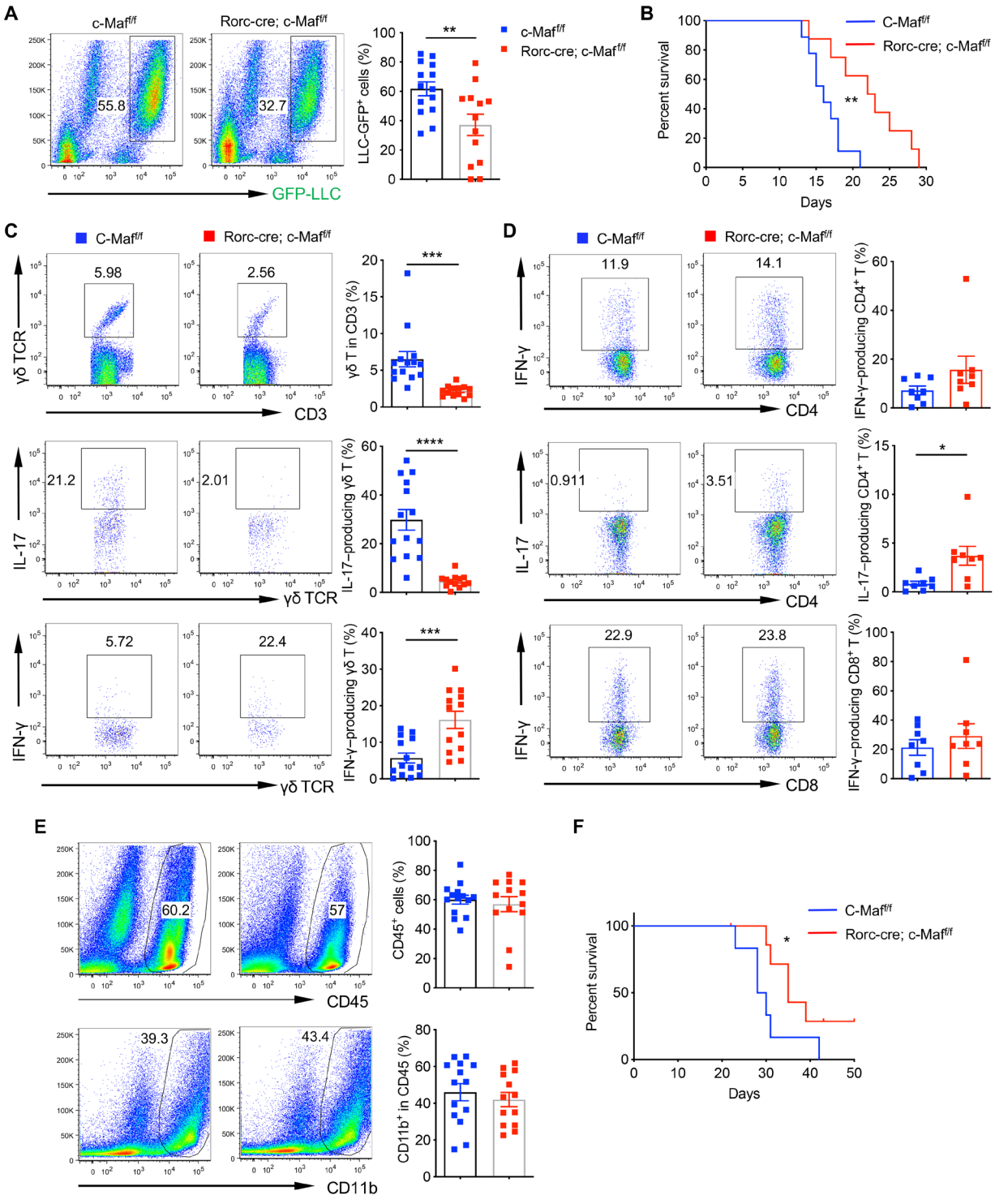


**Fig. 5. Deficiency of c-Maf in γδ T cells prolongs the overall survival in lung cancer metastasis models.** (**A**) Rorc-cre;c-Maf$^{f/f}$ and control c-Maf$^{f/f}$ mice were injected intravenously with LLC-GFP cells for 14 days. Tumor burden (%LLC-GFP) was assessed by flow cytometry. Summarized data are combined data from two independent studies. Each dot represents data from one mouse. (**B**) The overall survival of LLC-tumor bearing c-Maf$^{f/f}$ ($n = 9$) or Rorc-cre; c-Maf$^{f/f}$ mice ($n = 8$). (**C**) Percentages of γδ T cells in CD3$^+$ cells and IL-17– or IFN-γ–producing γδ T cells in the lung of LLC tumor model. Representative dot plots and summarized data are shown. (**D**) Intracellular IL-17 and IFN-γ production from CD4$^+$ T cells and IFN-γ production from CD8$^+$ T cells in the lungs of LLC tumor model. Representative dot plots and summarized data are shown. (**E**) Percentage of CD45$^+$ cells (%) (top) and percentage of CD11b$^+$ cells in CD45$^+$ cells (%) in the lung of LLC tumor model (bottom). Representative dot plots and summarized data are shown. (**F**) Survival of B16F10-bearing c-Maf$^{f/f}$ ($n = 6$) or Rorc-cre; c-Maf$^{f/f}$ ($n = 8$) mice. Data are represented as means ± SEM. *$P < 0.05$, **$P < 0.01$, ***$P < 0.001$, and ****$P < 0.0001$.

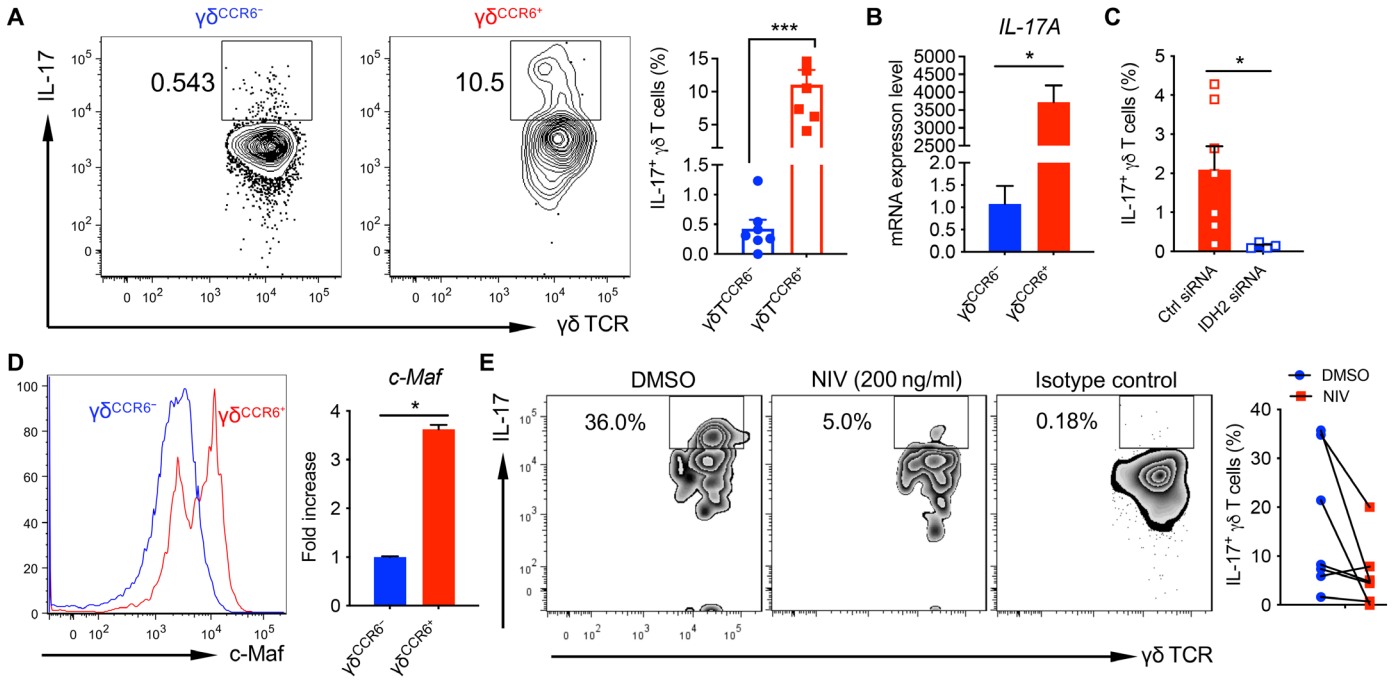


**Fig. 6. c-Maf is critical in regulating human polarized γδT17 cells.** (**A**) Intracellular IL-17 production in polarized CCR6$^-$ and CCR6$^+$ γδ T from human peripheral blood mononuclear cells (PBMCs) ($n = 6$). Representative dot plots and summarized data are shown. (**B**) The IL-17 mRNA expression levels in human polarized CCR6$^-$ and CCR6$^+$ γδ T by RT-PCR analysis. (**C**) Polarized γδ T cells from human PBMCs were transfected with control or IDH2 siRNA, and intracellular IL-17 was determined by flow cytometry. Summarized data are shown. (**D**) c-Maf expression in human CCR6$^-$ and CCR6$^+$ γδ T cells by flow cytometry (left) and RT-PCR analysis (right). (**E**) Human polarized CCR6$^+$ γδ T cells were treated with or without c-Maf inhibitor NIV, and intracellular IL-17 was detected by flow cytometry. Representative flow plots and summarized data are shown. Isotype control for IL-17 staining is also shown. Data are represented as means ± SEM. *$P < 0.05$ and ***$P < 0.001$.

while γδT17 use oxidative metabolism in mitochondria (*46*). Consistent with these studies, we found high expression of *glut1* and high glucose uptake in γδT1 cells. Inhibition of glycolysis by 2-DG reduced the production of IFN-γ from γδT1 but did not influence IL-17 production from γδT17 cells. We found that γδT17 cells may also rely on glutaminolysis in addition to OXPHOS pathway. High expression levels of metabolic enzyme genes including *GLS* and *GLUD1* that are involved in glutaminolysis were observed in γδT17 cells. In addition, α-KG, which is the critical metabolite linking TCA cycle and glutaminolysis, was also increased in γδT17 through an unbiased SIRM analysis. A recent study also demonstrated the critical role of glutamine metabolism in mouse γδT17 cells and skin inflammation (*29*, *30*). Further exploring the function of mitochondria, we observed differential levels of mitoROS in γδT17 and γδT1 cells. It has been reported that excessive ROS inhibits lung γδT17 cells (*47*). We observed a lower level of mitoROS intrinsically in γδT17 cells, while γδT1 cells have higher levels of mitoROS, which may be related to their antitumor effect. Inhibition of ROS significantly reduced IFN-γ production in γδT1 cells, further supporting this notion.

We have shown that differential metabolic activities play a critical role in the function of γδT1 and γδT17 cells. Intriguingly, we found a high expression level of metabolic enzyme IDH2 in γδT17, while γδT1 cells virtually do not express IDH2. Knockdown of IDH2 in γδT17 substantially decreased IL-17 production, while gain of function of IDH2 in γδT1 decreased the production of IFN-γ. These data suggest that IDH2 may function as a metabolic checkpoint regulating effector functions of γδ T subsets. IDH2 is mainly located in mitochondria and usually catalyzes isocitrate into α-KG in the TCA cycle. More carbon labeling in α-KG was seen in γδT17 cells compared to γδT1 cells. Deficiency of IDH2 in γδT1 cells may lead to a natural break in the transformation from isocitrate to α-KG. Furthermore, addition of exogenous α-KG significantly decreased IFN-γ production in γδT1 cells. These data identify IDH2 as a critical metabolic checkpoint regulating OXPHOS pathway in γδT17 cells and γδT1 effector function via shunting pyruvate into glycolysis pathway. IDH1 and IDH2 are also highly expressed in differentiated $T_H17$ cells (*48*). Knockdown of both IDH1 and IDH2 reduces IL-17A/F expression, suggesting a common metabolic pathway used by both $T_H17$ cells and innate γδT17 cells.

Interactions between transcription factor–mediated molecular mechanism and cellular metabolism determine T cell differentiation and effector function (*22*, *35*, *49*). Here, we found that transcription factor c-Maf was highly expressed in γδT17 cells and that c-Maf controls IL-17 production by directly interacting with IDH2, supporting the biological role of c-Maf in immune metabolism (*7*). It is worth noting that deficiency of c-Maf in CD27$^-$ γδ T cells did not affect the GLS and GLUD1 expression in these cells. These data suggest that c-Maf may regulate IL-17 production in γδ T cells independent of glutaminolysis (*30*). The mTOR signaling pathway has been shown to play a critical role in γδ T development and function (*31*, *33*, *34*). We found that mTORC2 deficiency resulted in reduced IL-17 production through regulation of c-Maf expression, suggesting that mTORC2 signaling is upstream of c-Maf. However, the detailed molecular regulatory mechanism needs to be elucidated in the future. In contrast, HIF-1α is dispensable for the function

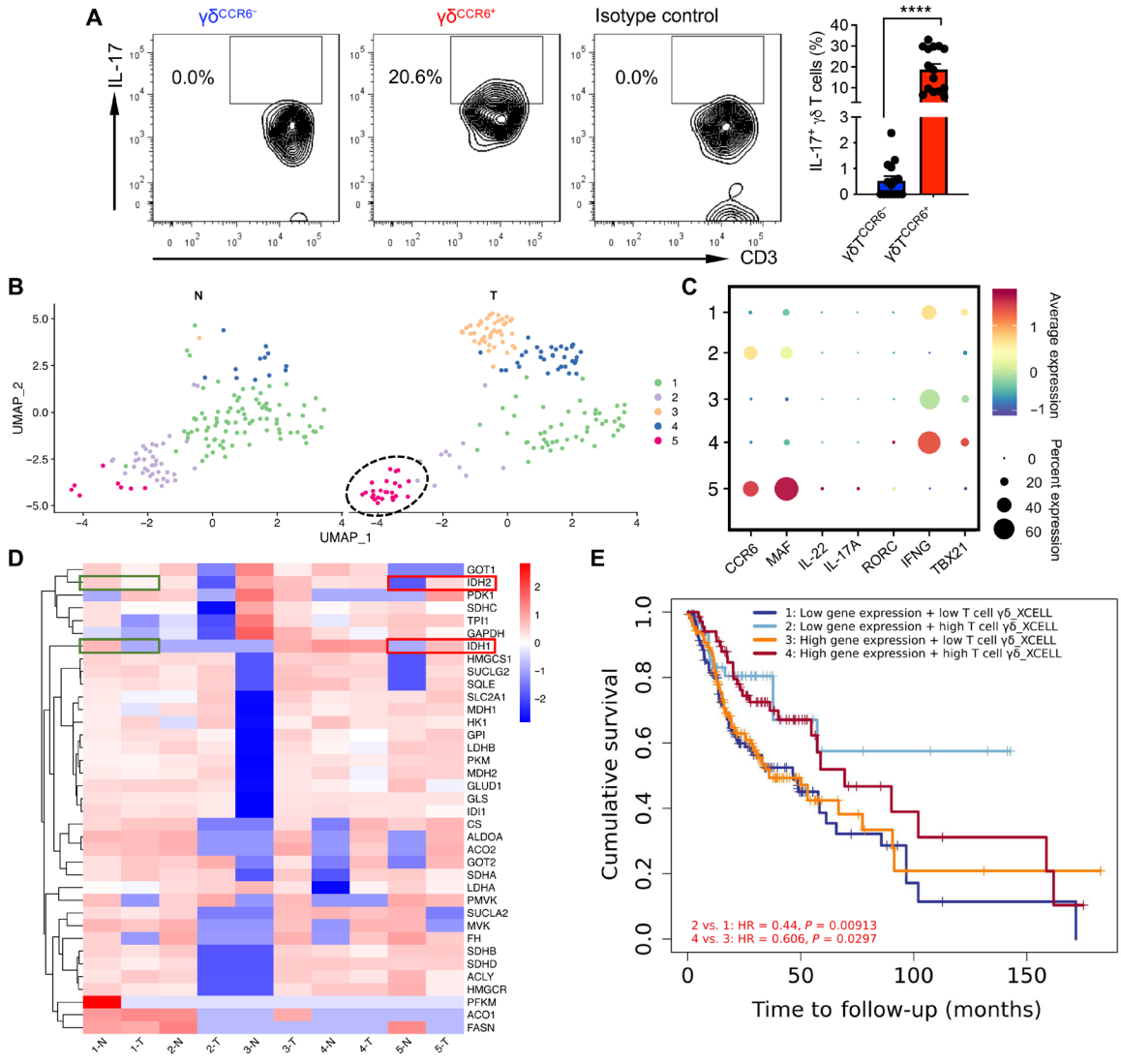


**Fig. 7. γδT17 cells in human oral tissues.** (**A**) Intracellular IL-17 production in human CCR6$^-$ and CCR6$^+$ γδ T from OSCC tissues by flow cytometry. Isotype control for IL-17 staining is also shown. Representative flow plots and summarized data are shown. Each dot represents data from one patient. (**B**) UMAP analysis from scRNA-seq data shows five γδ T cell clusters. The cluster 5 (circled) is more abundant in OSCC tissue (T) as compared to normal adjacent tissue (N). (**C**) Dot plots of gene expression in five clusters of γδ T cells from oral tissues. (**D**) Heatmaps of gene expression (metabolic enzymes) in five clusters of γδ T cells from adjacent normal tissue (N) and OSCC tissue (T). (**E**) Overall survival of patients with HNSC ($n = 522$) classified into four groups with differential c-Maf gene expression and γδ T cell infiltration. Group 1, low c-Maf expression and low γδ T cell infiltration; group 2, low c-Maf expression and high γδ T cell infiltration; group 3, high c-Maf expression and low γδ T cell infiltration; group 4, high c-Maf expression and high γδ T cell infiltration. HR, hazard ratio. Data are represented as means ± SEM. ****$P < 0.0001$.

and c-Maf expression in γδT17 cells. This is in contrast to $T_H17$ cells (*50*). Collectively, these results support the notion that transcription factor c-Maf plays a central role in γδT17 cells via the transcriptional and metabolic reprogramming.

Through the induction of an immunosuppressive tumor microenvironment, stimulation of angiogenesis, and restricting antitumor αβ T cell function, γδT17 have gained intensive investigation in various cancer types (*6*). In murine lung cancer, γδT17 were thought to be a potentially effective target for cancer treatment (*39*). It is hypothesized that inhibiting the transcription factor that controls IL-17 production in γδ T cells, such as RORγt, may serve as a promising approach. In this study, we observed significantly reduced IL-17 production in lung γδ T cells from c-Maf cKO mice. Consequently, c-Maf cKO mice exhibited prolonged survival in both LLC lung cancer model and B16F10 melanoma lung metastasis model. These results suggest that c-Maf is a promising target for cancer immunotherapy. Previously, we found that c-Maf is a checkpoint for reprogramming macrophages in lung cancer and that targeting c-Maf in myeloid cells leads to reduced tumor burden and enhanced antitumor immune response (*51*). Macrophages have been shown to play a critical role in promoting tumor progression and metastasis (*52*). Thus, developing previously unidentified approaches to target c-Maf in immunosuppressive macrophages and γδT17 cells may reverse their tumor-promoting effect while stimulating antitumor immunity, thereby controlling cancer progression and metastasis.

Although c-Maf has been identified as a critical transcription factor for murine γδT17 cells, it is unknown whether c-Maf also

regulates human γδT17 cells. Human γδT17 cells are scarce in the periphery, and they express CCR6. We found that c-Maf is highly expressed in CCR6$^+$γδ T cells and inhibition of c-Maf with a small-molecule inhibitor reduced IL-17 production, suggesting a potential role of c-Maf in human γδT17 cells. Similar as mouse γδ T cells, human γδ T cells are also enriched in mucosal tissues. We found a significant fraction of γδ T cells in oral tissues including OSCC tissues (*53*). Using scRNA-seq, we found five γδ T cell clusters and one particular cluster showed enriched gene expression of *MAF*, *CCR6*, *IL-22*, and *IL-17A*, suggesting a unique γδT17 gene signature. The abundance of this cluster also correlates with high expression levels of IDH1 and IDH2 in OSCC tissues, suggesting potential interactions between c-Maf– and IDH-mediated metabolism in human γδT17 cells. Silence or inhibition of IDH2 reduces IL-17 production in both polarized and primary human γδT17 cells. A recent elegant study using γδ T cells sorted from adult human peripheral blood and cord blood discovered type 1 effector γδ T cells that express *TBX21*, *FCGR3A*, and cytotoxicity-associated gene expression and type 3 effectors characterized by *CCR6*, *RORC*, *IL23R*, and *DPP4* expression (*54*). These type 1 and type 3 effector γδ T cells express similar gene signatures as γδT1 and γδT17 shown in our study. However, IL-17 was not detectable from type 3 effector γδ T cells, at least using flow cytometry (*54*). In our study, we did see considerable amount of IL-17 production from oral tissue infiltrating CCR6$^+$γδ T cells by flow cytometry. It is possible that oral tissue environment provides a specific set of cytokines/metabolites to endow IL-17 production (*53*), similar as γδT17 cells shown in human colon cancer (*42*) and pancreatic cancer (*55*). Patients with HNSC whose tumor had high infiltration of γδ T cells with low *c-MAF* gene expression but potentially high IFN-γ production showed significant better survival compared to those with high *c-MAF* gene expression regardless of high or low γδ T cell infiltration. These findings provide evidence to suggest that c-Maf also critically regulates human γδT17 cells in cancer potentially through metabolic reprogramming.

## MATERIALS AND METHODS

### Mice

Mice were housed and bred in the vivarium of clinical and translational research building (University of Louisville) under specific pathogen–free conditions. C57BL/6, c-Maf$^{f/f}$ and Rorc-cre; c-Maf$^{f/f}$, Raptor$^{f/f}$ and CD2-cre; Raptor$^{f/f}$, and Rictor$^{f/f}$ and CD2-cre; Rictor$^{f/f}$ mice aged between 6 and 8 weeks (both male and female) were used in experiments. c-Maf$^{f/f}$ mice were generated by Biocytogen (Beijing, China) and then were bred with Rorc-cre mice (022791, Jackson Laboratory) to generate c-Maf cKO mice. CD2-cre; Raptor$^{f/f}$ and CD2-cre; Rictor$^{f/f}$ mice were generated as previously reported (*31*). All these mice were on C57Bl/6 background and were both male and female mice (6 to 8 weeks old). All experiments involving animals were conducted in accordance with the ethical guidelines set by the University of Louisville Institutional Animal Care and Use Committee under the approved protocols 19471 and 19536.

### Preparation of a single-cell suspension and mouse γδ T cell polarization

A single-cell suspension was prepared from mouse LNs and spleens (both male and female mice, 6 to 8 weeks old). For the lung tissues, lungs were cut into small pieces and then digested for 20 min using digestion buffer containing collagenase IV, hyaluronidase, and deoxyribonuclease I. For γδT17 cell polarization, CD27$^-$ γδ T cells from LNs were cultured with IL-1β (10 ng/ml) and IL-23 (10 ng/ml) for 7 days in wells precoated with anti–γδ TCR monoclonal antibody (mAb) (clone: UC-7). For γδT1 cell polarization, sorted CD27$^+$ γδ T cells from pooled LNs and spleens were cultured with IL-2 (10 ng/ml) and IL-7 (10 ng/ml) for 7 days in wells precoated with anti-CD3 mAb (clone: 145-2C11). In some experiments, dimethyl 2-oxoglutarate (α-KG, Sigma-Aldrich), *N*-acetyl-L-cysteine (Sigma-Aldrich) were added during the culture. γδT17 and γδT1 cells were further sorted from cultures based on CD27 expression. Cells were sorted using FACSAria III cell sorter (BD Biosciences). The detailed commercial Ab information is listed in table S1.

### Intracellular staining and flow cytometry

Primary γδ T cells or polarized γδ T cells were stimulated with phorbol 12-myristate 13-acetate (PMA) and ionomycin in the presence of Golgi plug (BioLegend) for 4 hours or by IL-1β (10 ng/ml) and IL-23 (10 ng/ml) in the presence of Golgi plug (BioLegend) overnight at 37°C in complete RPMI 1640 medium. For some experiments, different concentrations of inhibitors were added as indicated. Small-molecule inhibitors including 2-DG, OXA, and AGI were purchased from Sigma-Aldrich. Cells were collected, surface-stained, fixed, and then intracellularly stained with fluorochrome-labeled mAbs against cytokines or transcription factors according to the manufacturer's instructions. Cells were acquired by FACSCanto II (BD Biosciences), and data were analyzed using FlowJo software (Tree Star).

### siRNA transfection and lentivirus infection in polarized mouse γδ T cells

Polarized CD27$^-$ γδ T cells were cultured in RPMI 1640 medium with 20% fetal bovine serum (FBS), and fluorescein isothiocyanate (FITC)–conjugated control siRNA (Santa Cruz Biotechnology, sc-36869) and IDH2 siRNA (Thermo Fisher Scientific, AM16708) were transfected with Lipofectamine 2000 (11668-027, Invitrogen). For the cytokine stimulation, cells were cultured for additional 24 hours with IL-1β (10 ng/ml) and IL-23 (10 ng/ml). The Golgi plug was added in the final 4 hours. For the PMA stimulation, cells were cultured for additional 24 hours and stimulated with PMA and ionomycin in the presence of Golgiplug (BioLegend) for 4 hours. Intracellular cytokine staining of IL-17 was performed. For lentivirus infection, polarized CD27$^+$ γδ T cells were cultured in complete RPMI 1640 medium with polybrene (8 μg/ml). Cells were infected with GFP-tagged blank lentivirus or IDH2 lentivirus (Applied Biological Materials Inc.) by centrifugation at the speed of 2300 rpm for 90 min at 30°C. Cells were then cultured in RPMI 1640 medium containing 20% FBS, IL-2 (10 ng/ml), and IL-7 (10 ng/ml). On the second day, GFP$^+$ γδ T cells were sorted and cultured for an additional 48 hours, and intracellular IFN-γ was examined.

### 2-NBDG uptake assay, MitoTracker Green/Red, and MitoSOX staining

Polarized γδ T cells were stained with 2-NBDG (Thermo Fisher Scientific) to determine the glucose uptake. MitoTracker Green/Red staining was performed as previously described (*31*) for the measurement of mitochondrial content. MitoSOX staining was performed to detect mitoROS release.

### Metabolomics analysis

For tracer and SIRM analyses, polarized CD27$^+$ and CD27$^-$ γδ T cells were cultured in glucose-free Dulbecco's modified Eagle's medium supplemented with 10 mM [U-$^{13}$C]-glucose and 10% dialyzed FBS for 24 hours. The cells were rinsed in cold phosphate-buffered saline (PBS) and quenched using a mixture containing 2 ml of acetonitrile and 1.5 ml of $H_2O$. After adding 1 ml of chloroform, the sample was homogenized and centrifuged at 3000 rpm, 4°C for 20 min. The top layer was transferred to a new tube and lyophilized. The dried sample was then dissolved in 100 μl of 20% acetonitrile and vigorously vortex-mixed for 3 min. After centrifugation at 14,000 rpm, 4°C for 20 min, the supernatant was collected for two-dimensional liquid chromatography–mass spectrometry (2DLC-MS) analysis. All samples were analyzed on a Thermo Q Exactive HF Hybrid Quadrupole-Orbitrap Mass Spectrometer coupled with a Thermo DIONEX UltiMate 3000 HPLC system (Thermo Fisher Scientific, Waltham, MA, USA). The UltiMate 3000 HPLC system was equipped with a reversed phase chromatography (RPC) column and a hydrophilic interaction chromatography (HILIC) column. The two columns were configured in parallel 2DLC mode.

For 2DLC separation, $H_2O$ with 0.1% formic acid was used as the mobile phase A for RPC and 10 mM ammonium acetate (pH 3.25) was used as the mobile phase A for HILIC. Acetonitrile with 0.1% formic acid was used as mobile phase B for both RPC and HILIC. To avoid systemic bias, the samples were analyzed by 2DLC-MS in a random order. All samples were first analyzed by 2DLC-MS positive mode followed by 2DLC-MS negative mode, to obtain the full MS data of each metabolite. A group-based pooled sample was prepared for quality control by mixing a small portion of the supernatant from all unlabeled samples in one group. One pooled sample was analyzed by 2DLC-MS after injection of every five biological samples. All pooled samples were also analyzed by 2DLC-MS/MS (tandem MS) in positive and negative mode respectively, to acquire MS/MS spectra of each metabolite at three collision energies (20, 40, and 60 eV).

MetSign software was used for spectrum deconvolution, metabolite identification, cross-sample peak list alignment, normalization, and statistical analysis (*56*, *57*). For a metabolite of interest with a poor chromatographic peak shape, its peak area was further validated using Xcalibur software (version 2.2 SP1; Thermo Fisher Scientific Inc., Germany). To identify metabolites, the 2DLC-MS/MS data of the pooled samples were first matched to an in-house MS/MS database that contains the parent ion mass/charge ratio ($m/z$), MS/MS spectra, and retention time of 205 metabolite standards. The thresholds used for metabolite identification were MS/MS spectral similarity $\geq 0.4$, retention time difference $\leq 0.15$ min, and $m/z$ difference $\leq 4$ ppm. The 2DLC-MS/MS data without a match in the in-house database were then analyzed using Compound Discoverer software (version 2.0; Thermo Fisher Scientific Inc., Germany), where the threshold of MS/MS spectrum similarity score was set as $\geq$40 with a maximum score of 100. The remaining peaks that did not have a match were then matched to the metabolites in the in-house MS/MS database using the parent ion $m/z$ and retention time to identify metabolites that do not have MS/MS spectra. The thresholds for assignment were parent ion $m/z \leq 4$ ppm and retention time difference $\leq 0.15$ min. The metabolomics data were deposited to Metabolomics Workbench with project ID: PR001313 (www.metabolomicsworkbench.org/data/DRCCMetadata.php?Mode=Project&ProjectID=PR001313).

### Western blot analysis

Sorted CD27$^+$ and CD27$^-$ γδ T cells were lysed in lysis buffer containing protease and phosphatase inhibitors. The cell lysates were then harvested and centrifuged at 14,000 rpm and 4°C for 15 min. The supernatants were then collected into separate 1.5-ml tubes and assayed for protein concentration using the Pierce BCA Protein Assay Kit (Thermo Fisher Scientific). The samples were further denatured and ran for SDS–polyacrylamide gel electrophoresis followed by transfer to polyvinylidene difluoride (PVDF) membrane. The PVDF membrane was blocked with 5% bovine serum albumin (BSA) in tris-buffered saline–Tween (TBST) solution for 1 hour at room temperature with shaking, washed with TBST three times for 10 min each, and stained for primary anti-HK1 (Cell Signaling Technology), PKM2 (Cell Signaling Technology), LDHA (Cell Signaling Technology), IDH1 (Aviva Systems Biology), IDH2 (Santa Cruz Biotechnology), and β-actin (Sigma-Aldrich) individually by incubating overnight at 4°C. The membranes were also blotted with primary Abs against enzymes critical in the TCA cycle (Tricarboxylic Acid Cycle Antibody Sampler Kit, Cell Signaling Technology). The membrane was then washed three times using 1× TBST for 10 min each, stained for secondary Abs, and incubated for 1 hour at room temperature followed by washing and addition of detection reagent (ECL plus Western Blotting Detection System, Amersham Biosciences).

### RNA extraction and RT-qPCR analysis

Sorted CD27$^+$ or CD27$^-$ γδ T cells were put in TRIzol, and RNA extraction was performed as previously described (*31*). Complementary DNA (cDNA) was synthetized with a reverse transcription kit (Bio-Rad), and RT-qPCR was then performed on a Bio-Rad CFX Connect Real-Time system (Bio-Rad) with SYBR Green (Bio-Rad). The primer sequences are listed in table S2.

### c-Maf ChIP-qPCR

In vitro polarized CD27$^-$ γδ T cells were used for ChIP studies. In brief, extracted chromatins were subjected to sonication using a sonicator [Adaptive Focused Acoustics (AFA) Focused ultrasonicator S220] to obtain chromatin fragments of 100 to 500 base pairs (bp). Fragmented chromatin was incubated with c-Maf Ab (LifeSpan BioSciences Inc.) or control normal rabbit immunoglobulin G (Cell Signaling Technology) overnight and then incubated with beads (Dynabeads Protein G, Invitrogen). Precipitated chromatins were reversed (65°C for 12 to 16 hours) and then purified using a QIAquick PCR purification kit (QIAGEN). ChIP-qPCR analysis was performed as described above. The primer sequences are listed in table S2.

### Mouse tumor models

c-Maf$^{f/f}$ and Rorc-cre; c-Maf$^{f/f}$ mice (6 to 8 weeks) were intravenously injected with GFP-tagged LLC cells ($4 \times 10^5$ per mouse). After 2 weeks, mice were euthanized, and tumor burden and immune cell phenotype in the lungs were examined. For survival study, mice were intravenously injected with LLC cells ($4 \times 10^5$ per mouse) or B16F10 cells ($1 \times 10^5$ per mouse). Mice were monitored up to 50 days after injection. LLC (CRL-1642) and B16F10 (CRL-6475) cells were originally purchased from American Type Culture Collection.

### Human PBMC isolation, human γδT17 in vitro expansion, and single-cell suspensions from oral cancer and adjacent tissues

Healthy donors were recruited to isolate peripheral blood mononuclear cells (PBMCs). PBMCs were cultured for 1 to 2 weeks in

complete RPMI 1640 medium with 10% FBS containing human IL-7 (20 ng/ml) in plates precoated with anti-human γδ TCR Ab (1 μg/ml) for the expansion of human γδT17 cells as previously reported (*41*). OSCC tissues and adjacent normal tissues were freshly collected from patients with OSCC in the Shanghai Ninth People's Hospital. Samples were subsequently minced on ice, followed by enzymatic digestion using type II collagenase (Sigma-Aldrich) with manual shaking every 5 min. Samples were then centrifuged at 300 relative centrifugal force (RCF) for 30 s at room temperature and removed the supernatant without disturbing the cell pellet. Next, 1× PBS (calcium and magnesium free) containing 0.04% BSA was added and then centrifugation at 300 RCF for 5 min. The cell pellet was resuspended in 1 ml of red blood cell lysis buffer and incubated for 10 min at 4°C. After lysis of red blood cells, samples were resuspended in 1 ml of PBS containing 0.04% BSA. Next, samples were filtered over 40-μm cell strainers (VWR) to obtain a single-cell suspension. Human participant study was approved by the Ethics Committee of the Shanghai Ninth People's Hospital, Shanghai, China.

### Human IDH2 siRNA knockdown and AGI inhibition

Polarized human γδ T cells were cultured in RPMI 1640 medium containing 20% FBS and then transfected with FITC-conjugated control siRNA (Santa Cruz Biotechnology, sc-36869) and IDH2 siRNA (Santa Cruz Biotechnology, sc-62487) with Lipo8000 reagent (Beyotime, C0533). A small amount of FITC-conjugated siRNA was also added into the IDH2 siRNA transfection well. Cells were cultured for additional 48 hours in RPMI 1640 medium with 10% FBS and IL-7 (10 ng/ml). For AGI inhibition assay, single-cell suspensions from oral cancer tissues were treated with varying concentrations of AGI (Sigma-Aldrich) or vehicle control dimethyl sulfoxide for 1 to 2 hours. Cells were stimulated with PMA and ionomycin in the presence of Golgi plug for 4 to 6 hours. Intracellular cytokine staining for IL-17 was performed.

### An scRNA-seq and data processing

Fresh OSCC and adjacent normal tissues ($n = 2$) were collected and processed into single-cell suspensions. Single-cell suspensions were loaded onto a Chromium single-cell controller instrument (10x Genomics) to generate single-cell gel beads in emulsions. Then, reverse transcription reactions were engaged to generate barcoded full-length cDNA, which was disrupted of emulsion by recovery agent. After cDNA cleanup, cDNA was amplified by PCR for appropriate cycles. Next, these amplified cDNA was fragmented, end-repaired, A-tailed, and ligated to an index adaptor, and then, the library was amplified. Every library was sequenced on a Hiseq X Ten platform (Illumina), and 150-bp paired-end reads were generated. The Cell Ranger software pipeline (version 3.1.0) provided by 10x Genomics was used to demultiplex cellular barcodes, map reads to the genome and transcriptome using the STAR aligner, and downsample reads as required to generate normalized aggregate data across samples, producing a matrix of gene counts versus cells.

The unique molecular identifier count matrix was processed using the R package Seurat (version 3.1.1). After applying quality control, single cells were included in downstream analyses, and library size normalization was performed with NormalizeData function in Seurat. Graph-based clustering was performed to cluster cells according to their gene expression profile using the FindClusters function in Seurat. The FindAllMarkers function (test.use = bimod) was used in Seurat to identify marker genes of each cluster. For a given cluster, FindAllMarkers identified positive markers compared with all other cells. Then, the R package SingleR, a novel computational method for unbiased cell type recognition of scRNA-seq, was applied with the reference transcriptomic datasets (Human Primary Cell Atlas) to infer the cell of origin of each of the single cells independently and identify cell types. Cells were visualized by RunUMAP, and differentially expressed genes were identified using the FindMarkers function (test.use = MAST) in Seurat. γδ T lineage genes including *TRDC*, *TRGC1*, and *TRDV2* were used to define γδ T cells. The scRNA-seq data were deposited to Gene Expression Omnibus (GEO) with access number 193766 (www.ncbi.nlm.nih.gov/geo/query/acc.cgi?acc=GSE193766).

### Outcome analysis of tumor-infiltrating γδ T cells and *c-MAF* gene expression

To further analyze the relationship between tumor-infiltrating γδ T cells and c-Maf gene expression levels, publicly available web platform TIMER (http://timer.cistrome.org) was used (*58*). The outcome mode was chosen to analyze the overall survival for patients with HNSC ($n = 522$, xCELL) with high or low γδ T cell infiltration with differential *c-MAF* gene expression levels.

### Statistical analysis

The data were processed by Prism 6 (GraphPad Software) and expressed as means ± SEM. The statistical analysis was performed using Prism 6 by Student's *t* test or one-way analysis of variance (ANOVA). Survival was analyzed by the Kaplan-Meier method. Differences were considered statistically significant when *P* value was less than 0.05.

## SUPPLEMENTARY MATERIALS

Supplementary material for this article is available at https://science.org/doi/10.1126/sciadv.abm9120

View/request a protocol for this paper from *Bio-protocol*.

## REFERENCES AND NOTES


1. S. Krishnan, I. E. Prise, K. Wemyss, L. P. Schenck, H. M. Bridgeman, F. A. McClure, T. Zangerle-Murray, C. O'Boyle, T. A. Barbera, F. Mahmood, D. M. E. Bowdish, D. M. W. Zaiss, J. R. Grainger, J. E. Konkel, Amphiregulin-producing γδ T cells are vital for safeguarding oral barrier immune homeostasis. *Proc. Natl. Acad. Sci. U.S.A.* **115**, 10738–10743 (2018).
2. C. A. Dillen, B. L. Pinsker, A. I. Marusina, A. A. Merleev, O. N. Farber, H. Liu, N. K. Archer, D. B. Lee, Y. Wang, R. V. Ortines, S. K. Lee, M. C. Marchitto, S. S. Cai, A. G. Ashbaugh, L. S. May, S. M. Holland, A. F. Freeman, L. G. Miller, M. R. Yeaman, S. I. Simon, J. D. Milner, E. Maverakis, L. S. Miller, Clonally expanded γδ T cells protect against Staphylococcus aureus skin reinfection. *J. Clin. Invest.* **128**, 1026–1042 (2018).
3. A. C. Hayday, γδ T cell update: Adaptate orchestrators of immune surveillance. *J. Immunol.* **203**, 311–320 (2019).
4. J. C. Ribot, A. deBarros, D. J. Pang, J. F. Neves, V. Peperzak, S. J. Roberts, M. Girardi, J. Borst, A. C. Hayday, D. J. Pennington, B. Silva-Santos, CD27 is a thymic determinant of the balance between interferon-gamma- and interleukin 17-producing gammadelta T cell subsets. *Nat. Immunol.* **10**, 427–436 (2009).
5. Y. Cai, X. Shen, C. Ding, C. Qi, K. Li, X. Li, V. R. Jala, H.-G. Zhang, T. Wang, J. Zheng, J. Yan, Pivotal role of dermal IL-17-producing γδ T cells in skin inflammation. *Immunity* **35**, 596–610 (2011).
6. C. Fleming, S. Morrissey, Y. Cai, J. Yan, γδ T cells: Unexpected regulators of cancer development and progression. *Trends Cancer* **3**, 561–570 (2017).
7. M. K. Zuberbuehler, M. E. Parker, J. D. Wheaton, J. R. Espinosa, H. R. Salzler, E. Park, M. Ciofani, The transcription factor c-Maf is essential for the commitment of IL-17-producing γδ T cells. *Nat. Immunol.* **20**, 73–85 (2019).
8. E. Moens, M. Brouwer, T. Dimova, M. Goldman, F. Willems, D. Vermijlen, IL-23R and TCR signaling drives the generation of neonatal Vγ9Vδ2 T cells expressing high levels of cytotoxic mediators and producing IFN-γ and IL-17. *J. Leukoc. Biol.* **89**, 743–752 (2011).

9. N. Caccamo, C. la Mendola, V. Orlando, S. Meraviglia, M. Todaro, G. Stassi, G. Sireci, J. J. Fournié, F. Dieli, Differentiation, phenotype, and function of interleukin-17-producing human Vγ9Vδ2 T cells. *Blood* **118**, 129–138 (2011).
10. Y. Cai, F. Xue, C. Quan, M. Qu, N. Liu, Y. Zhang, C. Fleming, X. Hu, H.-G. Zhang, R. Weichselbaum, Y.-X. Fu, D. Tieri, E. C. Rouchka, J. Zheng, J. Yan, A critical role of the IL-1β–IL-1R signaling pathway in skin inflammation and psoriasis pathogenesis. *J. Invest. Dermatol.* **139**, 146–156 (2019).
11. D. R. McKenzie, I. Comerford, B. Silva-Santos, S. R. McColl, The emerging complexity of γδT17 cells. *Front. Immunol.* **9**, 796 (2018).
12. J. D. Haas, F. H. M. González, S. Schmitz, V. Chennupati, L. Föhse, E. Kremmer, R. Förster, I. Prinz, CCR6 and NK1.1 distinguish between IL-17A and IFN-γ-producing γδ effector T cells. *Eur. J. Immunol.* **39**, 3488–3497 (2009).
13. K. Shibata, H. Yamada, T. Sato, T. Dejima, M. Nakamura, T. Ikawa, H. Hara, S. Yamasaki, R. Kageyama, Y. Iwakura, H. Kawamoto, H. Toh, Y. Yoshikai, Notch-Hes1 pathway is required for the development of IL-17-producing γδ T cells. *Blood* **118**, 586–593 (2011).
14. Y. Lu, X. Cao, X. Zhang, D. Kovalovsky, PLZF controls the development of fetal-derived IL-17+Vγ6+γδ T cells. *J. Immunol.* **195**, 4273–4281 (2015).
15. Y. Cai, F. Xue, C. Fleming, J. Yang, C. Ding, Y. Ma, M. Liu, H.-G. Zhang, J. Zheng, N. Xiong, J. Yan, Differential developmental requirement and peripheral regulation for dermal Vγ4 and Vγ6T17 cells in health and inflammation. *Nat. Commun.* **5**, 3986 (2014).
16. G. J. Fiala, B. Silva-Santos, How to develop IL-17-producing γδ T cells. *Immunol. Cell Biol.* **96**, 886–887 (2018).
17. R. Muro, T. Nitta, K. Nakano, T. Okamura, H. Takayanagi, H. Suzuki, γδTCR recruits the Syk/PI3K axis to drive proinflammatory differentiation program. *J. Clin. Invest.* **128**, 415–426 (2018).
18. P. H. Papotto, N. Gonçalves-Sousa, N. Schmolka, A. Iseppon, S. Mensurado, B. Stockinger, J. C. Ribot, B. Silva-Santos, IL-23 drives differentiation of peripheral γδ17 T cells from adult bone marrow-derived precursors. *EMBO Rep.* **18**, 1957–1967 (2017).
19. K. J. Ness-Schwickerath, C. Jin, C. T. Morita, Cytokine requirements for the differentiation and expansion of IL-17A- and IL-22-producing human Vγ2Vδ2 T cells. *J. Immunol.* **184**, 7268–7280 (2010).
20. K. Venken, P. Jacques, C. Mortier, M. E. Labadia, T. Decruy, J. Coudenys, K. Hoyt, A. L. Wayne, R. Hughes, M. Turner, S. van Gassen, L. Martens, D. Smith, C. Harcken, J. Wahle, C.-T. Wang, E. Verheugen, N. Schryvers, G. Varkas, H. Cypers, R. Wittoek, Y. Piette, L. Gyselbrecht, S. van Calenbergh, F. van den Bosch, Y. Saeys, G. Nabozny, D. Elewaut, RORγt inhibition selectively targets IL-17 producing iNKT and γδ-T cells enriched in Spondyloarthritis patients. *Nat. Commun.* **10**, 9 (2019).
21. R. P. Wilson, M. L. Ives, G. Rao, A. Lau, K. Payne, M. Kobayashi, P. D. Arkwright, J. Peake, M. Wong, S. Adelstein, J. M. Smart, M. A. French, D. A. Fulcher, C. Picard, J. Bustamante, S. Boisson-Dupuis, P. Gray, P. Stepensky, K. Warnatz, A. F. Freeman, J. Rossjohn, J. McCluskey, S. M. Holland, J.-L. Casanova, G. Uzel, C. S. Ma, S. G. Tangye, E. K. Deenick, STAT3 is a critical cell-intrinsic regulator of human unconventional T cell numbers and function. *J. Exp. Med.* **212**, 855–864 (2015).
22. R. Wang, C. P. Dillon, L. Z. Shi, S. Milasta, R. Carter, D. Finkelstein, L. L. McCormick, P. Fitzgerald, H. Chi, J. Munger, D. R. Green, The transcription factor Myc controls metabolic reprogramming upon T lymphocyte activation. *Immunity* **35**, 871–882 (2011).
23. K. Masui, K. Tanaka, D. Akhavan, I. Babic, B. Gini, T. Matsutani, A. Iwanami, F. Liu, G. R. Villa, Y. Gu, C. Campos, S. Zhu, H. Yang, W. H. Yong, T. F. Cloughesy, I. K. Mellinghoff, W. K. Cavenee, R. J. Shaw, P. S. Mischel, mTOR complex 2 controls glycolytic metabolism in glioblastoma through FoxO acetylation and upregulation of c-Myc. *Cell Metab.* **18**, 726–739 (2013).
24. L. Z. Shi, R. Wang, G. Huang, P. Vogel, G. Neale, D. R. Green, H. Chi, HIF1α-dependent glycolytic pathway orchestrates a metabolic checkpoint for the differentiation of TH17 and Treg cells. *J. Exp. Med.* **208**, 1367–1376 (2011).
25. K. N. Pollizzi, J. D. Powell, Integrating canonical and metabolic signalling programmes in the regulation of T cell responses. *Nat. Rev. Immunol.* **14**, 435–446 (2014).
26. E. L. Pearce, M. C. Poffenberger, C. H. Chang, R. G. Jones, Fueling immunity: Insights into metabolism and lymphocyte function. *Science* **342**, 1242454 (2013).
27. R. I. K. Geltink, R. L. Kyle, E. L. Pearce, Unraveling the complex interplay between T cell metabolism and function. *Annu. Rev. Immunol.* **36**, 461–488 (2018).
28. N. Lopes, C. McIntyre, S. Martin, M. Raverdeau, N. Sumaria, A. C. Kohlgruber, G. J. Fiala, L. Z. Agudelo, L. Dyck, H. Kane, A. Douglas, S. Cunningham, H. Prendeville, R. Loftus, C. Carmody, P. Pierre, M. Kellis, M. Brenner, R. J. Argüello, B. Silva-Santos, D. J. Pennington, L. Lynch, Distinct metabolic programs established in the thymus control effector functions of γδ T cell subsets in tumor microenvironments. *Nat. Immunol.* **22**, 179–192 (2021).
29. G. Li, L. Liu, Z. Yin, Z. Ye, N. Shen, Glutamine metabolism is essential for the production of IL-17A in γδ T cells and skin inflammation. *Tissue Cell* **71**, 101569 (2021).
30. X. Xia, G. Cao, G. Sun, L. Zhu, Y. Tian, Y. Song, C. Guo, X. Wang, J. Zhong, W. Zhou, P. Li, H. Zhang, J. Hao, Z. Li, L. Deng, Z. Yin, Y. Gao, GLS1-mediated glutaminolysis unbridled by MALT1 protease promotes psoriasis pathogenesis. *J. Clin. Invest.* **130**, 5180–5196 (2020).
31. Y. Cai, F. Xue, H. Qin, X. Chen, N. Liu, C. Fleming, X. Hu, H.-G. Zhang, F. Chen, J. Zheng, J. Yan, Differential roles of the mTOR-STAT3 signaling in dermal γδ T cell effector function in skin inflammation. *Cell Rep.* **27**, 3034–3048.e5 (2019).
32. R. Agerholm, J. Rizk, M. T. Vinals, V. Bekiaris, STAT3 but not STAT4 is critical for γδT17 cell responses and skin inflammation. *EMBO Rep.* **20**, e48647 (2019).
33. Q. Yang, X. Liu, Q. Liu, Z. Guan, J. Luo, G. Cao, R. Cai, Z. Li, Y. Xu, Z. Wu, M. Xu, S. Zhang, F. Zhang, H. Yang, X. Lin, M. Yang, Y. Wu, Y. Gao, R. Flavell, J. Hao, Z. Yin, Roles of mTORC1 and mTORC2 in controlling γδ T1 and γδ T17 differentiation and function. *Cell Death Differ.* **27**, 2248–2262 (2020).
34. K. Yang, D. B. Blanco, X. Chen, P. Dash, G. Neale, C. Rosencrance, J. Easton, W. Chen, C. Cheng, Y. Dhungana, A. Kc, W. Awad, X.-Z. J. Guo, P. G. Thomas, H. Chi, Metabolic signaling directs the reciprocal lineage decisions of αβ and γδ T cells. *Sci. Immunol.* **3**, eaas9818 (2018).
35. V. A. Gerriets, R. J. Kishton, A. G. Nichols, A. N. Macintyre, M. Inoue, O. Ilkayeva, P. S. Winter, X. Liu, B. Priyadharshini, M. E. Slawinska, L. Haeberli, C. Huck, L. A. Turka, K. C. Wood, L. P. Hale, P. A. Smith, M. A. Schneider, N. J. MacIver, J. W. Locasale, C. B. Newgard, M. L. Shinohara, J. C. Rathmell, Metabolic programming and PDHK1 control CD4+ T cell subsets and inflammation. *J. Clin. Invest.* **125**, 194–207 (2015).
36. H. Chi, Regulation and function of mTOR signalling in T cell fate decisions. *Nat. Rev. Immunol.* **12**, 325–338 (2012).
37. K. N. Pollizzi, J. D. Powell, Regulation of T cells by mTOR: The known knowns and the known unknowns. *Trends Immunol.* **36**, 13–20 (2015).
38. M. Bottcher, K. Renner, R. Berger, K. Mentz, S. Thomas, Z. E. Cardenas-Conejo, K. Dettmer, P. J. Oefner, A. Mackensen, M. Kreutz, D. Mougiakakos, D-2-hydroxyglutarate interferes with HIF-1α stability skewing T-cell metabolism towards oxidative phosphorylation and impairing Th17 polarization. *Onco. Targets. Ther.* **7**, e1445454 (2018).
39. C. Jin, G. K. Lagoudas, C. Zhao, S. Bullman, A. Bhutkar, B. Hu, S. Ameh, D. Sandel, X. S. Liang, S. Mazzilli, M. T. Whary, M. Meyerson, R. Germain, P. C. Blainey, J. G. Fox, T. Jacks, Commensal microbiota promote lung cancer development via γδ T cells. *Cell* **176**, 998–1013.e16 (2019).
40. B. Di Lorenzo, J. Dechanet-Merville, B. Silva-Santos, Peripheral clonal selection shapes the human γδ T-cell repertoire. *Cell. Mol. Immunol.* **14**, 733–735 (2017).
41. M. L. Michel, D. J. Pang, S. F. Y. Haque, A. J. Potocnik, D. J. Pennington, A. C. Hayday, Interleukin 7 (IL-7) selectively promotes mouse and human IL-17-producing γδ cells. *Proc. Natl. Acad. Sci. U.S.A.* **109**, 17549–17554 (2012).
42. P. Wu, D. Wu, C. Ni, J. Ye, W. Chen, G. Hu, Z. Wang, C. Wang, Z. Zhang, W. Xia, Z. Chen, K. Wang, T. Zhang, J. Xu, Y. Han, T. Zhang, X. Wu, J. Wang, W. Gong, S. Zheng, F. Qiu, J. Yan, J. Huang, γδT17 cells promote the accumulation and expansion of myeloid-derived suppressor cells in human colorectal cancer. *Immunity* **40**, 785–800 (2014).
43. S. Ma, Q. Cheng, Y. Cai, H. Gong, Y. Wu, X. Yu, L. Shi, D. Wu, C. Dong, H. Liu, IL-17A produced by γδ T cells promotes tumor growth in hepatocellular carcinoma. *Cancer Res.* **74**, 1969–1982 (2014).
44. M. Rei, N. Gonçalves-Sousa, T. Lança, R. G. Thompson, S. Mensurado, F. R. Balkwill, H. Kulbe, D. J. Pennington, B. Silva-Santos, Murine $CD27^{(-)}$ $Vγ6^{(+)}$ γδ T cells producing IL-17A promote ovarian cancer growth via mobilization of protumor small peritoneal macrophages. *Proc. Natl. Acad. Sci. U.S.A.* **111**, E3562–E3570 (2014).
45. S. B. Coffelt, K. Kersten, C. W. Doornebal, J. Weiden, K. Vrijland, C.-S. Hau, N. J. M. Verstegen, M. Ciampricotti, L. J. A. C. Hawinkels, J. Jonkers, K. E. de Visser, IL-17-producing γδ T cells and neutrophils conspire to promote breast cancer metastasis. *Nature* **522**, 345–348 (2015).
46. N. Lopes, B. Silva-Santos, Functional and metabolic dichotomy of murine γδ T cell subsets in cancer immunity. *Eur. J. Immunol.* **51**, 17–26 (2021).
47. D. Anthony, A. Papanicolaou, H. Wang, H. J. Seow, E. E. To, S. Yatmaz, G. P. Anderson, O. Wijburg, S. Selemidis, R. Vlahos, S. Bozinovski, Excessive reactive oxygen species inhibit $IL\text{-}17A^{+}$γδ T cells and innate cellular responses to bacterial lung infection. *Antioxid. Redox Signal.* **32**, 943–956 (2020).
48. T. Xu, K. M. Stewart, X. Wang, K. Liu, M. Xie, J. K. Ryu, K. Li, T. Ma, H. Wang, L. Ni, S. Zhu, N. Cao, D. Zhu, Y. Zhang, K. Akassoglou, C. Dong, E. M. Driggers, S. Ding, Metabolic control of TH17 and induced Treg cell balance by an epigenetic mechanism. *Nature* **548**, 228–233 (2017).
49. X. Chen, S. Morrissey, F. Chen, J. Yan, Novel insight into the molecular and metabolic mechanisms orchestrating IL-17 production in γδ T cells. *Front. Immunol.* **10**, 2828 (2019).
50. E. V. Dang, J. Barbi, H.-Y. Yang, D. Jinasena, H. Yu, Y. Zheng, Z. Bordman, J. Fu, Y. Kim, H.-R. Yen, W. Luo, K. Zeller, L. Shimoda, S. L. Topalian, G. L. Semenza, C. V. Dang, D. M. Pardoll, F. Pan, Control of $T_H17/T_{reg}$ balance by hypoxia-inducible factor 1. *Cell* **146**, 772–784 (2011).
51. M. Liu, Z. Tong, C. Ding, F. Luo, S. Wu, C. Wu, S. Albeituni, L. He, X. Hu, D. Tieri, E. C. Rouchka, M. Hamada, S. Takahashi, A. A. Gibb, G. Kloecker, H. G. Zhang, M. Bousamra II, B. G. Hill, X. Zhang, J. Yan, Transcription factor c-Maf is a checkpoint that programs macrophages in lung cancer. *J. Clin. Invest.* **130**, 2081–2096 (2020).
52. S. M. Morrissey, F. Zhang, C. Ding, D. E. Montoya-Durango, X. Hu, C. Yang, Z. Wang, F. Yuan, M. Fox, H.-G. Zhang, H. Guo, D. Tieri, M. Kong, C. T. Watson, R. A. Mitchell,

X. Zhang, K. M. McMasters, J. Huang, J. Yan, Tumor-derived exosomes drive immunosuppressive macrophages in a pre-metastatic niche through glycolytic dominant metabolic reprogramming. *Cell Metab.* **33**, 2040–2058.e10 (2021).
53. S. K. Sureshbabu, D. Chaukar, S. V. Chiplunkar, Hypoxia regulates the differentiation and anti-tumor effector functions of γδT cells in oral cancer. *Clin. Exp. Immunol.* **201**, 40–57 (2020).
54. L. Tan, A. S. Fichtner, E. Bruni, I. Odak, I. Sandrock, A. Bubke, A. Borchers, C. Schultze-Florey, C. Koenecke, R. Förster, M. Jarek, C. von Kaisenberg, A. Schulz, X. Chu, B. Zhang, Y. Li, U. Panzer, C. F. Krebs, S. Ravens, I. Prinz, A fetal wave of human type 3 effector γδ cells with restricted TCR diversity persists into adulthood. *Sci. Immunol.* **6**, eabf0125 (2021).
55. D. Daley, C. P. Zambirinis, L. Seifert, N. Akkad, N. Mohan, G. Werba, R. Barilla, A. Torres-Hernandez, M. Hundeyin, V. R. K. Mani, A. Avanzi, D. Tippens, R. Narayanan, J.-E. Jang, E. Newman, V. G. Pillarisetty, M. L. Dustin, D. Bar-Sagi, C. Hajdu, G. Miller, γδ T cells support pancreatic oncogenesis by restraining αβ T cell activation. *Cell* **166**, 1485–1499.e15 (2016).
56. X. Wei, W. Sun, X. Shi, I. Koo, B. Wang, J. Zhang, X. Yin, Y. Tang, B. Bogdanov, S. Kim, Z. Zhou, C. McClain, X. Zhang, MetSign: A computational platform for high-resolution mass spectrometry-based metabolomics. *Anal. Chem.* **83**, 7668–7675 (2011).
57. X. Wei, P. K. Lorkiewicz, B. Shi, J. K. Salabei, B. G. Hill, S. Kim, C. J. McClain, X. Zhang, Analysis of stable isotope assisted metabolomics data acquired by high resolution mass spectrometry. *Anal. Methods* **9**, 2275–2283 (2017).
58. T. Li, J. Fu, Z. Zeng, D. Cohen, J. Li, Q. Chen, B. Li, X. S. Liu, TIMER2.0 for analysis of tumor-infiltrating immune cells. *Nucleic Acids Res.* **48**, W509–W514 (2020).

**Acknowledgments:** We thank K. Wu and L. Zhong (Shanghai Ninth People's Hospital, Shanghai Jiao Tong University School of Medicine) for help in recruiting patients with OSCC. We also thank X. Yao, Q. Zi, and Q. Zu (Shanghai OE Biotech Co. Ltd.) for help in scRNA-seq analysis. **Funding:** This work was supported by the NIH (R01CA213990 and R01AI128818) and the Kentucky Lung Cancer Research Program (J.Y.). C.D. was supported by P20GM135004. This work was also supported by the NIH Instrument grant 1S10OD20106 (X.Z.). X.C. was supported by the China Scholarship Council (CSC no. 201806230234) and Shanghai Sailing Program (19YF1427500). **Author contributions:** Conceptualization: X.C., F.C., and J.Y. Methodology: X.C., Y.C., X.H., C.D., L.H., and X.Z. Investigation: X.C., Y.C., X.H., C.D., and L.H. Supervision: X.Z., F.C., and J.Y. Writing—original draft: X.C. and J.Y. Writing—review and editing: X.Z., F.C., and J.Y. **Competing interests:** The authors declare that they have no competing interests. **Data and materials availability:** All data needed to evaluate the conclusions in the paper are present in the paper and/or the Supplementary Materials. scRNA-seq data are available under GEO accession GSE193766. Metabolomics data are available on Metabolomics Workbench under project ID: PR001313.

Submitted 20 October 2021
Accepted 8 April 2022
Published 25 May 2022
10.1126/sciadv.abm9120